Auxetic hexachiral cantilever beams for piezoelectric vibration energy harvesting

Auxetic hexachiral cantilever beams for piezoelectric vibration energy harvesting

Shaik Sadikbasha[a], B. Radhika[b], V. Pandurangan[a*]

[a] Department of Mechanical Engineering, Indian Institute of Technology Tirupati, Tirupati, India
[b] Department of Civil and Environmental Engineering, Indian Institute of Technology Tirupati, Tirupati, India

Abstract

This work presents an auxetic hexachiral cantilever substrate for low-frequency vibration energy harvesting applications. Auxetics are materials with negative Poisson's ratio that develop stresses of the same nature under mechanical loading, which can be advantageously used in designing energy harvesters with enhanced power output. The proposed harvester is fabricated by attaching a piezo patch on a 3D printed polylactic acid (PLA) hexachiral substrate to convert the mechanical response to electrical output. Experiments are conducted to characterize the vibration and electrical properties of the harvester. A 3D finite element (FE) model is developed and validated with experimental voltage obtained for different electrical resistance. As the first mode generates maximum power, an equivalent single degree of freedom (SDOF) semi-analytical model is formulated and validated with experiments and FE results. The proposed harvester has a natural frequency of 23 Hz with a voltage output of 9.1 V at 250 kΩ. The developed models are used to study the influence of hexachiral geometry, electrical and mechanical loading on the electro-mechanical response. The harvester voltage is influenced by the ligament thickness and is found to increase linearly with an increase in mechanical loading. Further, the enhancement in performance by the addition of hexachiral sub patch to a plain beam is investigated, followed by a comparison with harvesters having plain, hexagonal and re-entrant geometries. The results show that the hexachiral harvester has the lowest first mode frequency with a power output about 20 and 3 times the plain and re-entrant harvesters, respectively. Finally, random vibration analysis of the hexachiral harvester is carried out to evaluate its performance under ambient loading, and the results show that the semi-analytical model is a computationally efficient alternative to study the first mode behavior. The findings of the study demonstrate the potential of the proposed hexachiral harvester for low-frequency applications.

Keywords: Vibration energy harvesters, Piezoelectric, Auxetic, Hexachiral, Negative Poisson's ratio, Random vibration.

1. Introduction

Low power sensors find applications in microelectronics, wireless technologies, smart devices, internet of things and structural health monitoring. Typically, these devices are powered by electrochemical batteries that have a shorter life, leakage issues and are difficult to dispose, which limits their use in critical applications [1]. Hence, self-powered wireless devices are highly sought in sensing, actuation, and wireless data transfer applications. Mechanical energy harvesters are helpful in such applications as they harness the energy from ambient sources such as vibrations, human body motion and heat, offering a sustainable alternative to batteries [2]. Fig. 1 shows the

*Corresponding author: raman@iittp.ac.in

range of operating frequencies for different mechanical systems that can be utilized in harvesting applications.

Vibration energy harvesters are widely used as vibration is a more commonly available source of energy [2]. They are broadly classified as electromagnetic, magnetostrictive, electrostatic and piezoelectric types based on their operating principle [3]. Among these, the electromagnetic and magnetostrictive energy harvesters are difficult to fabricate and integrate, while electrostatic harvesters need an external voltage source to generate an electric potential [4]. In contrast, piezoelectric energy harvesters (PEHs) are easily deployable, inexpensive, require lower maintenance, can be miniaturized and can generate power output from a few nanowatts to milliwatts, making them useful in self-powered wireless sensors used in medical and engineering applications [5]–[8]. PEH comprises of piezoelectric material, which is often mounted on a substrate that is in contact with the vibration source. The piezo material and substrate structure greatly influence the performance of the PEHs and, thus, widely studied over the years [1]. Among the different materials, piezoelectric ceramics are widely used as they are easy to manufacture, have stable power output, are compatible with MEMS, have higher efficiency and have low dielectric losses [9]–[11].

Piezoelectric vibration energy harvesters are broadly classified as resonant type and non-resonant impact type energy harvesters [11]. The performance of resonant type energy harvesters is largely dependent on the frequency, and their power output decreases significantly under non-resonant conditions. Non-resonant harvesters are frequency-independent and can operate over a large range of frequencies, but their power output and efficiency are lower compared to resonant type harvesters of the same size, and they also suffer from stability issues [12], [13]. Researchers have explored various substrate topologies, nonlinear methods and optimization techniques to improve the performance of resonant type harvesters [10], [14]. Yang et al. [15] proposed a curved piezoelectric energy harvester, which generates complex stress distributions along the excitation direction resulting in higher power output. Anton et al. [14] studied rectangular, triangular, trapezoidal, curved, and cymbal geometries and found that trapezoidal configuration generates higher power output due to uniform distribution of strains, whereas curved and cymbal designs achieve the same by distributing the loads. Dhote et al. [16] developed a multi-frequency harvester with nonlinear compliant springs having a wider operating bandwidth. However, higher operating frequencies and lower power output limit their use.

In order to improve the power output at low operating frequencies, Wang et al. [17] developed a bionic energy harvester inspired by a woodpeckers head structure for wearable devices with improved power density. Advances in 3D printing have enabled the fabrication of bioinspired and other substrates with cellular geometries that are lightweight and can be designed for low-frequency applications[18], [19]. A special class of cellular structures known as auxetics exhibit a negative Poisson's ratio, meaning they contract or expand laterally under compressive or tensile loading, unlike regular structures with a positive Poisson's ratio. The counterintuitive nature results in the same nature of stresses (compressive or tensile) along perpendicular directions, increasing the sum of mean axial and lateral components of stress tensor, yielding an improved power output. Apart from their auxetic nature, the change in geometry and deformations associated with auxetics result in stress concentration and geometric nonlinearity, which further improves the power output [20]. In their pioneering work on auxetic piezoelectrics, Muraoka et al. [21] developed an actuator based on the re-entrant geometry that amplified the displacements and also developed a theoretical model to estimate the displacement amplification and natural frequency. They also found that the auxetic geometry shows better amplification than structures with positive Poisson's ratio. In a

similar study, Fey et al. [22] fabricated auxetic re-entrant geometry using Lead Zirconate Titanate (PZT) ceramics and characterized their response under in-plane loading and found that the strains were amplified 30-70 times and the hydrostatic coefficient by 66 times compared to bulk PZT. The observations show a significant increase in piezoelectric coupling coefficients, which infer that auxetic piezo patches can significantly improve the power output compared to bulk PZTs. Topolov et al. [23] and Krishnaswamy et al. [24] developed lead-free auxetic polymer matrix composite piezo material with high piezoelectric sensitivity and large hydrostatic coefficients for energy harvesting applications, but their piezoelectric coupling coefficients are comparatively lower than PZTs resulting in lower power output. Kirigami inspired auxetic structures developed by Li et al. [25], and Farhangdoust et al. [26] showed an increase in power output by 2.76 and 19.2 times, respectively, compared to plain energy harvesters under the same operating conditions, but their conversion efficiencies are lower. Umino et al. [27] developed a re-entrant auxetic energy harvester for low-frequency applications and found a 10-70% shift in the natural frequency, charge density, and power output. Ferguson et al. [28] proposed an auxetic piezoelectric energy harvester for increased power output by harnessing the strain vibration and investigated the influence of glue strength on peak stress, which remained the same regardless of strength. Eghbali et al. [20], [29] and Farhangdoust et al. [30] proposed auxetic boosters and circular auxetic energy harvesters to enhance the performance and found that using auxetic re-entrant sub patch on plain substrate improved power output by 3-7 times. Chen et al. [31], [32] proposed a nonlinear re-entrant harvester with lumped mass that improved power output and operating bandwidth by 2-4 times and 15-20 times, respectively. They also showed that auxetic substrates improve efficiency and operating bandwidth, which are functions of substrate topology.

The design of vibration energy harvesters has evolved over the years yet requiring the development of low-frequency harvesters for small scale applications. Existing designs that operate at lower frequencies have poor efficiencies and low power output, restricting their use in practical applications [20]. Studies on auxetic substrate energy harvesters are in the nascent stage and are mostly limited to re-entrant geometries. A particular class of auxetics known as chiral structures exhibit negative Poisson's ratio through the rolling and unrolling action of ligaments around circular or rectangular nodes. Chiral structures convert large strains to small strains by using the coupled rotation and translation deformation [33]. Laura et al. [34] developed a piezoelectric strain sensor using the auxetic anti-tetra chiral structure and found that the auxetic sensor has better sensitivity than the square lattice structure and accurately captures small strains. However, the use of chiral structures in vibration energy harvesters has not been explored.

In this context, the study addresses some of these aspects by proposing a lightweight auxetic hexachiral structure that exhibits axial–rotation and uniform deformations over large strains for applications in low-frequency vibration energy harvesting. The major contributions from this study are (a) the design and characterization of an hexachiral vibration energy harvester for low-frequency applications and (b) the development of finite element (FE) and semi-analytical models to predict the proposed harvester performance. The study will also address questions on a) the influence of substrate structure on the coupled electro-mechanical response of the harvester, which is relevant both to optimize the design and to improve the efficiency of an already installed harvester, b) performance of proposed harvester compared to those having re-entrant, hexagonal and plain beam geometries to highlight its superior performance c) performance of the harvester under random loading, which is more representative of the loads experienced in the field.

The paper is organized as follows: in section 2, the design of the hexachiral energy harvester is explained along with the working principle and section 3 presents characterization studies. In

section 4, FE and semi-analytical models of the proposed harvester are presented, using which in section 5, parametric studies and aspects related to improving efficiency and comparing performance with respect to other geometries are discussed. Section 6 presents the response of the hexachiral energy harvester to random loads, and finally, section 7 provides a summary and conclusions from the study.

2. Working principle and design of hexachiral energy harvester

The proposed vibration energy harvester with the axis convention and piezo patch arrangement is shown in Fig. 2. It consists of a 3D printed polylactic acid (PLA) substrate, one end of which is modified to the hexachiral geometry as shown in Fig. 2(a). A piezo patch consisting of a brass plate with ceramic PZT is bonded to the hexachiral region of the substrate (Fig. 2(b)). The dimensions of the hexachiral substrate and piezo patch are given in both Fig. 3 and Table 1. The dimensions of the substrate are chosen to suit the diameter of the commercially available piezo patch. The length of substrate used in harvesting applications are typically in the range of 10-100 mm, with the length being at least twice the width of the piezo patch, to allow bending of the substrate and harvest sufficient power [1]. As the piezo patch used in this study is 35 mm in diameter, the overall length of the substrate is chosen as 80 mm, with a 35 mm auxetic region to match the sub patch dimensions.

The hexachiral unit cell consists of a circular node at the centre with six tangential ligaments. The ratio of node radius to ligament length is maintained at 5 to ensure adequate distance between nodes and to allow a bending dominant response [35]. The hexachiral structure exhibits in-plane isotropy and uniform negative Poisson's ratio over a large range of strains [35]. To demonstrate the auxetic behavior of the substrate with the hexachiral unit cell, a finite element (FE) model is developed and analyzed under different loading conditions. The substrate, shown in Fig. 2(a), is modelled in Creo and imported to Abaqus for further analysis. It is fixed at one end and subjected to tensile, compressive, and bending loads at the free end after discretization using S4R elements, and the deformed shapes are shown in Fig. 4. The uniaxial compression causes inward rolling of ligaments, leading to the inward material flow in the attached piezo patch resulting in the same kind of in-plane stresses. Similar in-plane deformation showing the ligament unrolling in tension and inward rolling under bending around circular nodes is observed. The average normal stress distribution in the piezo patch along axes 1 and 2 under uniaxial compression is shown in Fig. 5, and it can be observed that the in-plane stresses are of the same nature. This may be attributed to the inward pull of the material caused by the rolling action of ligaments, as shown in Fig. 4, confirming the auxetic nature.

Piezoelectric materials consist of asymmetric dipole crystals, which get polarized under externally applied load and generate an electric potential that is proportional to the applied load. The coupled electro-mechanical response of piezoelectric materials is governed by the following constitutive equation [28]:

$$\begin{pmatrix} S \\ D \end{pmatrix} = \begin{pmatrix} S^E & d' \\ d & \varepsilon^T \end{pmatrix} \begin{pmatrix} T \\ E \end{pmatrix} \tag{1}$$

where $S, D, T,$ and $E,$ respectively, correspond to the strain, charge density, stress vector and electric field, and S^E compliance under constant electric field, ε^T dielectric permittivity under constant stress. The parameters d', d are converse and direct piezoelectric effect matrices, respectively, and the superscript $'$ denotes matrix transpose. From Eq. (1), it may be noted that the

generated electric field is proportional to stresses and strains developed in the piezoelectric material. As the stresses developed in the piezo material are small when using the linear theory of piezoelectric materials, the electric charge density can be related to stress in the PZT as

$$D_i = d_{ij}\sigma_j; i = 1, 2, 3 \tag{2}$$

where σ_j is the j^{th} component of the stress vector T. The harvester is assumed to undergo bending about the 2-axis, causing it to stretch along the longitudinal direction and generating an electric field in the piezo patch, which is polarized along the 3-axis or in the thickness direction. The charge density in the piezo patch of the energy harvester can be derived from Eq. (2) as

$$D_3 = d_{31}\sigma_1 + d_{32}\sigma_2 + d_{33}\sigma_3 \tag{3}$$

For an isotropic material under plane stress conditions $\sigma_3 = 0$ and $d_{31} = d_{32}$ and therefore, Eq. (3) reduces to the form

$$D_3 = d_{31}(\sigma_1 + \sigma_2) \tag{4}$$

The power output of a harvester is proportional to the square of the charge density and can be obtained from Eq. (4) as [26],

$$P \propto d_{31}(\sigma_1 + \sigma_2)^2 \tag{5}$$

For plane stress conditions, Eqs. (4) and (5) can be rewritten in terms of strains as

$$D_3 = d_{31}\frac{E}{1-\nu}(\varepsilon_1 + \varepsilon_2) \tag{6}$$

$$P \propto (\varepsilon_1 + \varepsilon_2)^2 \tag{7}$$

From Eq. (5), it is evident that the power output is higher when the in-plane stresses are of the same nature, which is true for the hexachiral substrate discussed earlier. This can also be shown as follows. For small deformations, the generalized Hooke's law can be used to describe the stress-strain relationship of the hexachiral structure as

$$\sigma_{ij} = C_{ijkl}\varepsilon_{kl} \tag{8}$$

Under plane stress conditions, and considering the Poisson's ratio to be -1, Eq. (8) can be rewritten in the following form

$$\begin{aligned} \epsilon_1 &= \tfrac{1}{E}(\sigma_1 - \nu\sigma_2) = \tfrac{1}{E}(\sigma_1 + \sigma_2) \\ \epsilon_2 &= \tfrac{1}{E}(\sigma_2 - \nu\sigma_1) = \tfrac{1}{E}(\sigma_1 + \sigma_2) \end{aligned} \tag{9}$$

Substituting the above expressions in Eq. (7) yields,

$$P \propto \frac{4(\sigma_1 + \sigma_2)^2}{E^2} \tag{10}$$

As the hexachiral structure exhibits a negative Poisson's ratio over a large range of strains, it can be incorporated into the harvester design to improve its power output.
The hexachiral substrate used in this study is made from PLA and is 3D printed in a Stratasys machine having an accuracy of 20-microns. A 45º raster orientation is used while printing as it provides better strength [36]. The piezo patch is bonded over the auxetic region, as shown in Fig. 2(b). Vibration energy harvesters are generally used in the cantilever mode as mounting is simple and generates higher deflection compared to fixed-fixed or propped configurations, which translates to higher power output. Hence, in the following sections, a systematic characterization study is carried out to evaluate the frequencies and power output of the proposed hexachiral energy harvester in the cantilever mode. Subsequently, FE and semi-analytical models are developed, which are validated with experimental results for predicting the power output and for use in parametric studies.

3. Experimental characterization of hexachiral energy harvester

In the first phase of the study, the hexachiral energy harvester is experimentally characterized for mechanical and electrical responses under different loading conditions. As the fabricated specimen is lightweight and small, it is difficult to carry out impact hammer tests to determine natural frequencies. Thus, the harvester is mounted on a Modal shop 2100E11 shaker capable of providing 440 N peak force excitation with 25.4 mm stroke in the range of 2-5400 Hz. Most of the conventional vibration energy harvesters are characterized in the cantilever mode owing to ease in mounting. Hence, the specimen is sandwiched between clamping plates and fastened to the plunger of the shaker using bolts to enable testing in cantilever mode. The shaker is connected to the 2100E18 amplifier, which drives the shaker with continuous gain adjustments to modulate the signal strength and amplitude. The amplifier is further connected to OROS 38 that houses the signal generator, data acquisition system and signal controller. The OROS 38 controller uses NV gate software for real-time analysis and post-processing of the output. Harmonic excitations of constant acceleration amplitude are provided through the controller to characterize the dynamic response of the hexachiral energy harvester. A PCB piezotronics accelerometer with a sensitivity of 5.33 mV/m/s^2 is mounted on the shaker head to measure the vibration amplitude. The complete experimental setup is shown in Fig. 6. The piezo patch is connected to an external variable resistor with a range of 0.001-500 kΩ representing the electrical load. The output from the piezo patch is connected to Tektronix DPO 2004B digital phosphor oscilloscope using a voltage probe having 10X attenuation to visualize and measure the voltage across the resistors. The harvester is first subjected to sine sweep at constant excitation amplitude to determine the natural frequencies, and the subsequent experiments are carried out at the first mode of natural frequency to investigate the influence of resistance and acceleration amplitude on the measured power output.
The experiments are repeated on three hexachiral specimens under the same operating conditions to ensure repeatability, and the first mode natural frequencies of the three samples are 22, 24, and 22 Hz. The small variation in the frequencies is expected, considering that there can be variations in mass during the fabrication. Hence, for further comparison, the natural frequency of the harvester is taken to be 22 Hz. The vibration energy equivalent in terms of acceleration from

common sources such as car engine compartments, portable air compressors, and domestic appliances is typically in the range of 0.1 to 15 m/s^2 [37]. Hence, the samples are subjected to sinusoidal base excitation of 15 m/s^2 at their corresponding first mode natural frequencies, and the voltage output is measured by varying the electrical resistance from 0.1-500 kΩ.
The voltage outputs for the three samples measured using the oscilloscope are presented in Fig. 7(a). It can be observed that the voltage drop across the resistors increases until the external resistance matches with the internal impedance of the piezo patch and decreases thereafter. Initially, the current flow increases with external load resulting in a higher voltage drop, but when the external load resistance is more than internal impedance, the current flow reduces, resulting in a lower voltage drop across the resistor. The maximum voltage of 9.1 V is observed at 250 kΩ. Fig. 7 (a) also shows the average voltage obtained from the three trials and the corresponding polynomial fit to the data. The electrical power output computed using average voltage, and the corresponding resistance is shown in Fig. 7(b). The hexachiral energy harvester generated 352 µW power in the resonant condition. Further, a finite element model is developed to predict the performance of the hexachiral energy harvester at higher modes and understand the influence of geometry, load, deformation modes, and electrical response.

4. Models for hexachiral energy harvester

4.1 Finite element model

The hexachiral energy harvester is modelled in Creo and imported into COMSOL Multiphysics 5.4 to solve the coupled multiphysics problem. The exploded view of the harvester shown in Fig. 8 consists of a PLA substrate with hexachiral geometry, adhesive layer, and brass plate to which the piezoceramic layer is bonded. The mechanical properties of the PLA material, presented in Table 2, are obtained from tensile tests on 3D printed specimens. The tests are carried out as per ASTM D638 [38] in a 100 kN MTS universal testing machine in displacement-controlled mode. The properties of the epoxy adhesive and brass substrate are taken from the supplier data and literature [20]. The properties of the piezo patch, which are important in determining the electrical response from the model, are also obtained from the manufacturer's catalogue. After a systematic mesh convergence study, the computational domain is discretized using 233460 tetrahedron and triangle-based swept mesh elements.
As discussed in section 2, the energy harvester exhibits electro-mechanical characteristics as described in Eq. (1). Hence, multiphysics analysis is carried out in COMSOL by coupling the solid mechanics module with electrostatic analysis. The model shown in Fig. 8 is fixed at one end to simulate the clamped condition, and a thin elastic layer boundary condition with a stiffness of 50 GPa/m is used to simulate the epoxy bonding of 30-micron thickness between the substrate and piezo patch. The piezoelectric elements enforce charge conservation boundary conditions for the electrostatic analysis. One side of the piezo patch is grounded, and the other side is modelled as a terminal, which are integral to the electrical circuit. The circuit is formed by connecting the resistor to the external I terminal and ground to simulate the external electrical load in the COMSOL. The voltage drop is measured across the two resistor pins connected to the piezo patch and later used to compute the power output, completing the development of the FE model.
The model is first validated using primary mechanical and electrical quantities from the experiments, which are the natural frequencies and the output voltage, respectively. The validated model is further used to a) investigate the influence of ligament thickness, base excitation acceleration, and external resistance on the voltage and power output, b) compare the performance

of a hexachiral sub patch added to a plain beam harvester under different loading conditions and arrive at an optimal sub patch thickness for maximum power output, c) compare the performance of the proposed harvester with geometrically similar harvesters of other substrates in use, and d) evaluate the response of the hexachiral energy harvester under random loading to simulate field conditions.

4.1.1 Validation and characterization of the harvester

The finite element model is validated by comparing both the mechanical (natural frequencies) and electrical (voltage across different resistors) responses from the experiments. Initially, the modal analysis is carried out to determine the natural frequencies, followed by frequency domain analysis to characterize the harvester at different operating conditions. The first mode frequency from the FE model is 23 Hz which agrees with the experimental value of 22 Hz within a 5% error. The damping ratio does have an influence on the results of the FE model and is dependent on the raster orientation used in 3D printing. In this study, a damping ratio of 1% is used, based on the dissipation factor for PLA materials available in the literature [36]. The finite element results are obtained for all resistances in the range 0.001-500 kΩ in increments of 0.001 kΩ, while the experimental results are obtained at a few representative resistance values within the range as shown in Fig. 7(a). It may be observed that the voltage obtained from the FE model is proportional to resistance up to 75 kΩ, after which the increase is gradual and reaches a maximum of 9.2 V at 250 kΩ. An additional increase in resistance causes a drop in voltage due to lower current flows. The energy dissipation in the form of heat causes a large current flow leading to a linear voltage drop across the resistor. A further increase in resistance leads to more energy dissipation and a drop in voltage across the resistor. The voltage predicted by the FE model agrees with the experimental data except at a few instances in the vicinity of optimum resistance. However, the error is 13% near optimal resistance and is within 5% elsewhere, which attests the accuracy of the FE model. The power output P, is obtained from the load resistance R and the root mean square value of voltage V_{rms} as

$$P = \frac{V_{rms}^2}{R} \tag{11}$$

Fig. 7(b) shows powers obtained from experiments and the FE model at different resistance values. A correlation of 0.76 is observed between the experimental and FE model, further validating the latter. Further, the efficiency of the harvester can be computed as [39],

$$\eta = \frac{\frac{V_{rms}^2}{R}}{\frac{1}{2} m \times \ddot{x}_a \times \dot{x}_a} \tag{12}$$

where, $m, \ddot{x}_a$, and $\dot{x}_a$ are mass, acceleration and velocity amplitudes, respectively. The input mechanical energy to the system denoted by the denominator in Eq. (12) for the acceleration amplitude of 15 m/s^2 was obtained as 38.5 mW, which translates to an efficiency of 1.03%. This metric is particularly useful when the design of the harvester has to be optimized for a particular

application. The validated model is used to characterize the hexachiral energy harvester at higher modes.

The validated model is used to characterize the hexachiral energy harvester at higher modes.

The study investigated response of the energy harvester at higher modes that are less than 200 Hz, which is typical in low and medium frequency applications. Thus, the first four frequencies and modes shapes of the hexachiral energy harvester are presented in Fig. 9. The first bending mode with a natural frequency of 23 Hz results in maximum voltage output due to the higher stresses experienced by the structure. The second and third mode shapes are translational and torsional modes, while the fourth is also a bending mode, which is expected for a cantilever beam. The voltages harvested in all these modes are in the order of 1×10^{-3} V, which are significantly lower than the first mode, as the stresses in the auxetic substrates at higher modes are lower. For comparison, the maximum stress in the auxetic substrate in the four modes are 30, 0.8, 0.04 and 0.035 MPa, respectively. Hence, in the remaining part of the study, only the first natural frequency is considered for electrical characterization and power computation.

4.2 Semi-analytical model

A single degree of freedom (SODF) lumped mass model is proposed for the first mode behavior of the harvester to estimate the natural frequency and voltage, as shown in Fig. 10. As seen in the figure, the piezoelectric element is treated as an equivalent voltage source connected in parallel to internal capacitance and external resistor**.** The mass of the harvester is assumed to be lumped at the intersection of the auxetic region and solid beam to obtain the voltage in the piezo patch. The governing equations for predicting the coupled electro-mechanical response of the piezoelectric energy harvesters are [32],

$$m\ddot{x}(t) + c\dot{x}(t) + kx(t) + \theta v(t) = -m\ddot{z}(t) \tag{13a}$$

$$c_p\dot{v}(t) + \frac{v(t)}{R} - \theta\dot{x}(t)=0 \tag{13b}$$

where $\ddot{z}(t)$ is the base acceleration, $m, c, k, \theta, v, c_p, R$ represent lumped mass, damping coefficient, equivalent stiffness, piezoelectric coupling coefficient, voltage, internal capacitance, and electrical resistance, respectively, and x is the displacement of lumped mass m relative to the base. The capacitance c_p and the coupling coefficient θ are related to material properties given by [40],

$$c_p = \frac{\left(\varepsilon_{33} - \frac{d_{31}^2}{S_{11}^E}\right)A}{h} \tag{14}$$

$$\theta = \frac{eA}{h} \tag{15}$$

where $e, h, A,$ and S_{11}^E are piezoelectric coupling coefficient, thickness, area of the piezo patch and component of the compliance tensor S^E, respectively. As the hexachiral substrate geometry is complex, it is difficult to analytically compute the equivalent stiffness k in Eq. (13a). Hence, the stiffness of the hexachiral substrate is obtained from the FE model, and its value along with other parameters used in the SDOF model are given in Table 3. The governing equations of the electro-

mechanical system (Eqs. (13)) can be solved analytically and numerically using ode45 solver in MATLAB. The amplitude of the voltage for harmonic base excitation is given by [41],

$$V(\Omega) = H(\Omega)\, Z(\Omega) \tag{16}$$

$$H(\Omega) = -\frac{i\Omega^3 \left(\frac{\alpha\theta}{c_p}\right)}{\Delta_1(\Omega)} \tag{17}$$

$$\Omega = \frac{\omega}{\omega_n} \text{ and } \alpha = \omega_n c_p R \tag{18}$$

$$\Delta_1(\Omega) = (i\Omega)^3\alpha + (2\zeta\alpha + 1)(i\Omega)^2 + (\alpha + \kappa^2\alpha + 2\zeta)(i\Omega) + 1 \tag{19}$$

$$\kappa^2 = \frac{\theta^2}{k c_p} \tag{20}$$

$$\omega_n = \sqrt{\frac{k}{m}} \text{ and } \zeta = \frac{c}{2m\omega_n} \tag{21}$$

where, $V(\Omega)$ and $Z(\Omega)$ are voltage and base displacement in frequency domain, defined in terms of non-dimensional parameter $\Omega = \frac{\omega}{\omega_n}$. The natural frequency of 21.6 Hz obtained from the SDOF model shows good agreement with the experimental result of 22 Hz, with an error of less than 2%. Further, the resistance is varied from 0.001–500 kΩ to obtain the electrical response at 21.6 Hz. Fig. 11 compares the voltage from experiments and SDOF model at resistance values of 150, 200, 250 and 300 kΩ, where a slight phase shift can be observed due to the difference in the natural frequencies. Fig. 12 compares the absolute voltage obtained from the SDOF (analytical and numerical) and FE models. The voltage from the SDOF model shows an increment up to 400 kΩ and with further increase in resistance, the voltage reaches an asymptotic value of about 12.5 V, as observed in FE results. Fig. 13 shows the output voltage from the FE and SDOF models for different base excitation loads, and it can be noted that both the models agree well with experimental results with an error of less than 12 %. The figure shows a linear relation between base excitation load and output voltage, which is expected as the stresses are directly proportional to the excitation load.

5. Studies on hexachiral energy harvester

5.1 Parametric analysis using the validated FE model

The thickness of the ligament in the hexachiral unit cell influences its stiffness, auxetic response and mass, which in turn affects the electro-mechanical response of the harvester. Hence, a parametric study is carried out to investigate the influence of ligament thickness on the electro-

mechanical response and arrive at the optimum ligament thickness. The thickness of the ligament in the chiral unit cell is varied from 0.675 to 1.5 mm. A thickness increase beyond 1.5 mm will result in a solid beam without auxetic nature, hence larger thicknesses are not considered. The results of the FE simulation are summarized in Table 4, which shows the variation of mass, stiffness, and natural frequencies for different ligament thicknesses. It is observed that the natural frequency of the harvester increases from 23 Hz to 32 Hz with increasing thickness due to an increase in stiffness. This leads to a corresponding drop in output voltage and power, as seen in Fig. 14 (a) and (b), respectively. The maximum voltage corresponding to ligament thickness of 0.675, 1, 1.25 and 1.50 mm are 9.2, 7.2, 6.5, and 4.5 V, respectively. The corresponding power outputs are 397, 285, 218 and 156 μW, at the optimal resistance of 154, 150, 150 and 100 kΩ, respectively. The results show a 41% increase in natural frequency and a 50% drop in the corresponding output voltage across the resistor.

The harvester can experience a range of excitation levels in field applications depending on the operating environment. A parametric study is carried for base excitation levels ranging from 0.1 – 15 m/s^2, mimicking field conditions, to assess the performance of the harvester under different working conditions. Fig. 15 (a) and (b) show the voltage and power at different excitation levels and for different ligament thicknesses, where it is observed that voltage increases linearly with acceleration levels.

Further, the thickness of the various layers in the sensor also influences the power output of the harvester, which is generally governed by the stresses developed and the leakage current. To examine this influence, the harvester was analysed with a PZT layer of 0.2 mm for the values of brass plate thickness reported in Table 5. With the increase in thickness the natural frequency increased from 17.2 Hz to 25.5 Hz because of the increase in the overall stiffness of the system. When the thickness is below 0.2 mm, the stresses in the harvester are higher than the limiting values, while for higher thicknesses, there is a decrease in the power output owing to increased stiffness. Next, the PZT layer thickness was varied for a constant brass plate thickness of 0.3 m and the results are shown in Table 5. While the lower power output for thicknesses less than 0.1 mm is due to leakage current, at higher values, it is due to stiffer sections. However, the sensor design is also influenced by fabrication process parameters and the requirements from a particular application, which are not within the scope of the present study.

5.2 Characterization of plain energy harvester with hexachiral sub patch

In applications where a plain beam energy harvester is already installed, its efficiency can be improved by bonding hexachiral sub patches, as shown in Fig. 16. The addition of the hexachiral sub patch amplifies the displacements, thereby enhancing the power output compared to a plain beam energy harvester. In order to investigate the performance of plain energy harvester with the sub patch, 0.25, 0.50, 1 and 2 mm thick sub patches are bonded on a plain beam of 2 mm thickness and modal analysis is carried out to determine the natural frequencies. The addition of hexachiral sub patch reduces the natural frequency of the plain beam by 11.6% for the thinnest sub patch, as seen in Table 6. The reduction in natural frequency is due to the increase in mass of the harvester. Further, analysis is carried out at corresponding first mode natural frequencies to find the voltage and power output with the addition of sub patch. Fig. 17 shows the voltage and power output variation for different sub patch thicknesses across different resistance. The maximum power of 17.5 μW is obtained for a 0.25 mm thick sub patch at 66 kΩ at the corresponding voltage of 1.1 V. The results show that sub patch increases power output of plain energy harvester for the smallest

sub patch thickness of 0.25 mm by 16% due to displacement amplification. However, at higher thickness, the increase in power output is not significant.

5.3 Influence of substrate geometry on the performance of energy harvester

The performance of the hexachiral energy harvester is also compared with geometrically similar plain beams, cellular non-auxetic and auxetic harvesters. The study considered conventional plain beam, hexagonal, and re-entrant substrates, and a plain beam with hexachiral sub patch as shown in Fig. 18. The FE models of the different geometries are analyzed in COMSOL for the same loads and cantilever boundary condition, and the results are summarized in Table 7**.** The results show that the natural frequencies for harvesters with cellular substrate designs are at least about 50% lower than the plain beam harvester of the same size. Further, among the cellular substrates, the hexachiral harvester has the lowest frequency of 23 Hz, which makes it well suited for low-frequency applications. Fig. 19 shows the variation of voltage and power across different resistance for all the configurations. Again, the results show that the voltage and power output are higher for harvesters with cellular geometries, which may be attributed to the fact that the displacement amplification in cellular geometries are higher. Among them, auxetic hexachiral substrate shows a higher power output of 397 μW, which is 3 and 20 times higher than re-entrant and plain beam configurations, respectively. The hexachiral geometry with 1.5 mm thick ligaments generates 10% more power output than the re-entrant substrate, and its first mode natural frequency is also lower, making it a good choice in energy harvesting applications.

6. Random vibration analysis of the harvester

The proposed FE and SDOF models of the harvester are subjected to random loading to analyze their performance for ambient conditions. Depending on the source, random loads are characterized by the power spectral density (PSD) functions indicating the average power in the signal at various frequencies. The ambient vibrations are typically bandlimited signals with either a narrow or wide spectrum. To evaluate the performance of the harvester, two typical cases of variable and constant PSDs for the base acceleration are considered, with the latter representing a white noise input to the system. The form of the PSDs are given by,

$$S_{\ddot{z}\ddot{z}}(\omega) = B\left(\frac{\beta}{\beta^2 + (\omega - 1)^2} + \frac{\beta}{\beta^2 + (\omega + 1)^2}\right) \tag{22}$$

$$S_{\ddot{z}\ddot{z}}(\omega) = I \tag{23}$$

where $B, \beta,$ and I are constants. In both cases, the base acceleration is assumed to be a stationary Gaussian random process, and samples of the corresponding time histories are simulated using the following equation.

$$\ddot{z}(t) = \sum_{i=1}^{N}[a_i \cos(\omega_i t) + b_i \sin(\omega_i t)] \tag{24}$$

where a_i and b_i are zero mean independent Gaussian random variables with variance $\sigma_i^2 = S_{\ddot{z}\ddot{z}}(\omega_i)$, for the i^{th} frequency with N being the total number of points considered in the frequency scale.

In the analysis $B = 2 \times 10^4 m^2, \beta = 500$, and $I = 2 \times 10^3 m^2$ are assumed so that the maximum base acceleration will be about 15 m/s^2. A good match between the PSD estimated and target PSD using the simulated samples is observed as shown in Fig. *20* (a) and (b) for variable and constant PSD, respectively. The FE model of the harvester is analyzed for an ensemble of base accelerations and the PSD of the voltage response for both the cases are estimated as shown in Fig. 21 (a) and (b) for the variable and constant PSDs, respectively. For the linear SDOF model of the harvester, a closed-form solution for the voltage PSD can be obtained as [41],

$$S_{\mathrm{vv}}(\omega) = |H(\omega)|^2 \frac{S_{\ddot{z}\ddot{z}}(\omega)}{\omega^4} \tag{25}$$

Eqs. (13a) and (13b) are also numerically analyzed for the samples of base acceleration. The analytical and numerical estimates of the voltage PSD are also shown in Fig. 21 and are observed to closely match the FE model results. Once again, as the power is observed to be distributed around the first natural frequency of the harvester, the SDOF model is a good representation for the harvester in this mode. Further, using kth order moments(M_k) of voltage PSD, the mean (μ_1) and variance (σ^2) are computed for different cases using Eqs. (26) – (28) as[42],

$$M_k = \frac{\int_0^\infty \omega^k S_{\mathrm{vv}}(\omega) d\omega}{\int_0^\infty S_{\mathrm{vv}}(\omega) d\omega} \tag{26}$$

$$\mu_1 = M_1 \tag{27}$$

$$\sigma^2 = M_2 - \mu_1^2 \tag{28}$$

The estimated mean and variance of the voltage PSD from the SDOF numerical and analytical analyses are found to compare well with the FE estimates as shown in Table 8. A higher value from FE analysis is observed owing to the contribution from the second mode within the considered frequency range. Moreover, the computation time for the analysis of the FE model for a single sample of base acceleration is noted to be 2.5 hours while the same for the numerical analysis of the SDOF model is 67 s. Hence, the SDOF model is a computationally efficient alternative for the proposed harvester when closed-form solutions are not feasible.

7. Conclusions

This study investigated the performance of auxetic hexachiral substrate for low-frequency energy harvesting applications. FE and SDOF models were developed to estimate the natural frequencies and power output of the harvester, and the results were validated with experiments. Parametric studies were carried out to assess the performance of the harvester under different operating conditions. Further additional studies comparing the performance of the proposed harvester with geometrically similar structures were carried out. Also, studies were performed to highlight the merit of the auxetic nature of the proposed harvester and the associated model in practical applications. The following are the major conclusions from the study:

(i) The proposed hexachiral energy harvester has a natural frequency of 23 Hz and corresponding voltage output of 9.2 V at 250 kΩ. The maximum power output was observed to be 397 μW at an optimal resistance of 154 kΩ.

(ii) Ligament thickness alters the stiffness of the harvester, thereby influencing the electro-mechanical response. Increasing the ligament thickness from 0.675 mm to 1.5 mm resulted in a 41% increase in natural frequency and a 50% drop in the corresponding voltage output across the resistor. Further, the voltage and base acceleration were observed to have a linear relationship.

(iii) The addition of a hexachiral sub patch to a plain beam harvester enhances its power output. In this study, the addition of a 0.25 mm sub patch to a 2 mm substrate increased its power output by 16%.

(iv) Energy harvesters with cellular geometries exhibit lower first mode frequencies than plane beam harvesters. Among them, the hexachiral energy harvester had the lowest frequency. This, combined with the fact that it generates the maximum power output, shows its potential for low-frequency applications.

(v) Auxetic substrates, in general, show better performance than other cellular or plain beam geometries. Particularly, the power output of the hexachiral harvester (397 μW) is about 20 and 3 times that of the plain beam and re-entrant harvesters, respectively.

(vi) The SDOF model is a computationally efficient alternative for studies on the proposed energy harvester, specifically in the first mode.

The results of this study are expected to provide better insights into vibration energy harvesters with cellular auxetic geometries and the design of energy harvesters for a typical application.

Acknowledgements

The first and third authors acknowledge the financial support from the Science and Engineering Research Board, Government of India under project grant CRG/2020/003369.

References

[1] Z. Yang, S. Zhou, J. Zu, and D. Inman, "High-Performance Piezoelectric Energy Harvesters and Their Applications," *Joule*, vol. 2, no. 4, pp. 642–697, 2018, doi: 10.1016/j.joule.2018.03.011.

[2] C. Covaci and A. Gontean, "Piezoelectric energy harvesting solutions: A review," *Sensors (Switzerland)*, vol. 20, no. 12, pp. 1–37, 2020, doi: 10.3390/s20123512.

[3] W. Zhou, D. Du, Q. Cui, C. Lu, Y. Wang, and Q. He, "Recent Research Progress in Piezoelectric Vibration Energy Harvesting Technology," *Energies 2022, Vol. 15, Page 947*, vol. 15, no. 3, p. 947, Jan. 2022, doi: 10.3390/EN15030947.

[4] A. Mohanty, S. Parida, R. K. Behera, and T. Roy, "Vibration energy harvesting: A review," *J. Adv. Dielectr.*, vol. 9, no. 4, pp. 1–17, 2019, doi: 10.1142/S2010135X19300019.

[5] S. Priya, "Advances in energy harvesting using low profile piezoelectric transducers," *J. Electroceramics*, vol. 19, no. 1, pp. 165–182, 2007, doi: 10.1007/s10832-007-9043-4.

[6] H. Salehi, R. Burgueño, S. Chakrabartty, N. Lajnef, and A. H. Alavi, "A comprehensive review of self-powered sensors in civil infrastructure: State-of-the-art and future research trends," *Eng. Struct.*, vol. 234, no. August 2020, p. 111963, May 2021, doi: 10.1016/j.engstruct.2021.111963.

[7] Y. Liu *et al.*, "Piezoelectric energy harvesting for self-powered wearable upper limb applications," *Nano Sel.*, vol. 2, no. 8, pp. 1459–1479, Aug. 2021, doi: 10.1002/nano.202000242.

[8] S. Roundy and P. K. Wright, "A piezoelectric vibration based generator for wireless electronics," *Smart Mater. Struct.*, vol. 13, no. 5, pp. 1131–1142, 2004, doi: 10.1088/0964-1726/13/5/018.

[9] H. Liu, J. Zhong, C. Lee, S. W. Lee, and L. Lin, "A comprehensive review on piezoelectric energy harvesting technology: Materials, mechanisms, and applications," *Appl. Phys. Rev.*, vol. 5, no. 4, 2018, doi: 10.1063/1.5074184.

[10] M. Safaei, H. A. Sodano, and S. R. Anton, "A review of energy harvesting using piezoelectric materials: State-of-the-art a decade later (2008-2018)," *Smart Mater. Struct.*, vol. 28, no. 11, 2019, doi: 10.1088/1361-665X/ab36e4.

[11] N. Sezer and M. Koç, "A comprehensive review on the state-of-the-art of piezoelectric energy harvesting," *Nano Energy*, vol. 80, p. 105567, Feb. 2021, doi: 10.1016/J.NANOEN.2020.105567.

[12] T. Yang, S. Zhou, S. Fang, W. Qin, and D. J. Inman, "Nonlinear vibration energy harvesting and vibration suppression technologies: Designs, analysis, and applications," *Appl. Phys. Rev.*, vol. 8, no. 3, p. 031317, Sep. 2021, doi: 10.1063/5.0051432.

[13] A. Hosseinkhani, D. Younesian, P. Eghbali, A. Moayedizadeh, and A. Fassih, "Sound and vibration energy harvesting for railway applications: A review on linear and nonlinear techniques," *Energy Reports*, vol. 7, pp. 852–874, Nov. 2021, doi: 10.1016/j.egyr.2021.01.087.

[14] S. R. Anton and H. A. Sodano, "A review of power harvesting using piezoelectric materials (2003-2006)," *Smart Mater. Struct.*, vol. 16, no. 3, 2007, doi: 10.1088/0964-1726/16/3/R01.

[15] Z. Yang, Y. Q. Wang, L. Zuo, and J. Zu, "Introducing arc-shaped piezoelectric elements

into energy harvesters," *Energy Convers. Manag.*, vol. 148, pp. 260–266, 2017, doi: 10.1016/J.ENCONMAN.2017.05.073.

[16] S. Dhote, H. Li, and Z. Yang, "Multi-frequency responses of compliant orthoplanar spring designs for widening the bandwidth of piezoelectric energy harvesters," *Int. J. Mech. Sci.*, vol. 157–158, pp. 684–691, Jul. 2019, doi: 10.1016/J.IJMECSCI.2019.04.029.

[17] B. Wang, Z. Long, Y. Hong, Q. Pan, W. Lin, and Z. Yang, "Woodpecker-mimic two-layer band energy harvester with a piezoelectric array for powering wrist-worn wearables," *Nano Energy*, vol. 89, Nov. 2021, doi: 10.1016/J.NANOEN.2021.106385.

[18] S. Iyer, M. Alkhader, and T. A. Venkatesh, "Electromechanical response of piezoelectric honeycomb foam structures," *J. Am. Ceram. Soc.*, vol. 97, no. 3, pp. 826–834, 2014, doi: 10.1111/jace.12699.

[19] N. Chandrasekharan and L. L. Thompson, "Increased power to weight ratio of piezoelectric energy harvesters through integration of cellular honeycomb structures," *Smart Mater. Struct.*, vol. 25, no. 4, p. 0, 2016, doi: 10.1088/0964-1726/25/4/045019.

[20] P. Eghbali, D. Younesian, A. Moayedizadeh, and M. Ranjbar, "Study in circular auxetic structures for efficiency enhancement in piezoelectric vibration energy harvesting," *Sci. Rep.*, vol. 10, no. 1, pp. 1–11, 2020, doi: 10.1038/s41598-020-73425-1.

[21] M. Muraoka and S. Sanada, "Displacement amplifier for piezoelectric actuator based on honeycomb link mechanism," *Sensors Actuators, A Phys.*, vol. 157, no. 1, pp. 84–90, Jan. 2010, doi: 10.1016/j.sna.2009.10.024.

[22] T. Fey *et al.*, "Mechanical and electrical strain response of a piezoelectric auxetic PZT lattice structure," *Smart Mater. Struct.*, vol. 25, no. 1, p. 015017, Dec. 2015, doi: 10.1088/0964-1726/25/1/015017.

[23] V. Y. Topolov and C. R. Bowen, "High-performance 1–3-type lead-free piezo-composites with auxetic polyethylene matrices," *Mater. Lett.*, vol. 142, pp. 265–268, Mar. 2015, doi: 10.1016/J.MATLET.2014.12.018.

[24] J. A. Krishnaswamy, F. C. Buroni, R. Melnik, L. Rodriguez-Tembleque, and A. Saez, "Design of polymeric auxetic matrices for improved mechanical coupling in lead-free piezocomposites," *Smart Mater. Struct.*, vol. 29, no. 5, p. 054002, Apr. 2020, doi: 10.1088/1361-665X/ab7e35.

[25] Q. Li, Y. Kuang, and M. Zhu, "Auxetic piezoelectric energy harvesters for increased electric power output," *AIP Adv.*, vol. 7, no. 1, pp. 1–5, Jan. 2017, doi: 10.1063/1.4974310.

[26] S. Farhangdoust, G. Georgeson, J.-B. B. Ihn, and F.-K. K. Chang, "Kirigami auxetic structure for high efficiency power harvesting in self-powered and wireless structural health monitoring systems," *Smart Mater. Struct.*, vol. 30, no. 1, p. 015037, Dec. 2020, doi: 10.1088/1361-665X/abcaaf.

[27] Y. Umino, T. Tsukamoto, S. Shiomi, K. Yamada, and T. Suzuki, "Development of vibration energy harvester with 2D mechanical metamaterial structure," *J. Phys. Conf. Ser.*, vol. 1052, no. 1, 2018, doi: 10.1088/1742-6596/1052/1/012103.

[28] W. J. G. Ferguson, Y. Kuang, K. E. Evans, C. W. Smith, and M. Zhu, "Auxetic structure for increased power output of strain vibration energy harvester," *Sensors Actuators, A Phys.*, vol. 282, pp. 90–96, Oct. 2018, doi: 10.1016/j.sna.2018.09.019.

[29] P. Eghbali, D. Younesian, and S. Farhangdoust, "Enhancement of piezoelectric vibration energy harvesting with auxetic boosters," *Int. J. Energy Res.*, vol. 44, no. 2, pp. 1179–1190, Feb. 2020, doi: 10.1002/ER.5010.

[30] S. Farhangdoust, G. Georgeson, J.-B. Ihn, and A. Mehrabi, "Embedded Metamaterial Subframe Patch for Increased Power Output of Piezoelectric Energy Harvesters," *J. Nondestruct. Eval. Diagnostics Progn. Eng. Syst.*, vol. 5, no. 1, pp. 1–6, 2022, doi: 10.1115/1.4051492.

[31] K. Chen, S. Fang, Q. Gao, D. Zou, J. Cao, and W.-H. Liao, "An enhanced nonlinear piezoelectric energy harvester with multiple rotating square unit cells," *Mech. Syst. Signal Process.*, vol. 173, p. 109065, Jul. 2022, doi: 10.1016/J.YMSSP.2022.109065.

[32] K. Chen, Q. Gao, S. Fang, D. Zou, Z. Yang, and W. H. Liao, "An auxetic nonlinear piezoelectric energy harvester for enhancing efficiency and bandwidth," *Appl. Energy*, vol. 298, no. June, p. 117274, Sep. 2021, doi: 10.1016/j.apenergy.2021.117274.

[33] F. Scarpa, S. Blain, T. Lew, D. Perrott, M. Ruzzene, and J. R. Yates, "Elastic buckling of hexagonal chiral cell honeycombs," *Compos. Part A Appl. Sci. Manuf.*, vol. 38, no. 2, pp. 280–289, Feb. 2007, doi: 10.1016/j.compositesa.2006.04.007.

[34] M. L. De Bellis and A. Bacigalupo, "Auxetic behavior and acoustic properties of microstructured piezoelectric strain sensors," *Smart Mater. Struct.*, vol. 26, no. 8, 2017, doi: 10.1088/1361-665X/aa7772.

[35] D. Prall and R. S. Lakes, "Properties of chiral honeycombe with Poisson's ratio of -1," *Int. J. Mech. Sci*, vol. 39, no. 3, 1997.

[36] X. He, M. Qu, and X. Shi, "Damping Properties of Ethylene-Vinyl Acetate Rubber/Polylactic Acid Blends," *J. Mater. Sci. Chem. Eng.*, vol. 04, no. 03, pp. 15–22, 2016, doi: 10.4236/msce.2016.43003.

[37] T. B. Xu, *Energy harvesting using piezoelectric materials in aerospace structures*. 2016. doi: 10.1016/B978-0-08-100148-6.00007-X.

[38] ASTM, "Standard Test Method for Tensile Properties of Plastics 1," 2006. doi: 10.1520/D0638-14.1.

[39] Z. Yang, A. Erturk, and J. Zu, "On the efficiency of piezoelectric energy harvesters," *Extrem. Mech. Lett.*, vol. 15, pp. 26–37, Sep. 2017, doi: 10.1016/J.EML.2017.05.002.

[40] J. J. Dosch, D. J. Inman, and E. Garcia, "A Self-Sensing Piezoelectric Actuator for Collocated Control," *J. Intell. Mater. Syst. Struct.*, vol. 3, no. 1, pp. 166–185, 1992, doi: 10.1177/1045389X9200300109.

[41] S. Adhikari, M. I. Friswell, and D. J. Inman, "Piezoelectric energy harvesting from broadband random vibrations," *Smart Mater. Struct.*, vol. 18, no. 11, 2009, doi: 10.1088/0964-1726/18/11/115005.

[42] B. Saltzberg, W. . Burton, J. . Barlow, and N. . Burch, "Moments of the power spectral density estimated from samples of the autocorrelation function (a robust procedure for monitoring changes in the statistical properties of lengthy non-stationary time series such as the EEG," *Electroencephalogr. Clin. Neurophysiol.*, vol. 61, pp. 89–93, 1985, doi: 10.1308/rcsann.2013.95.7.533a.

List of Figures

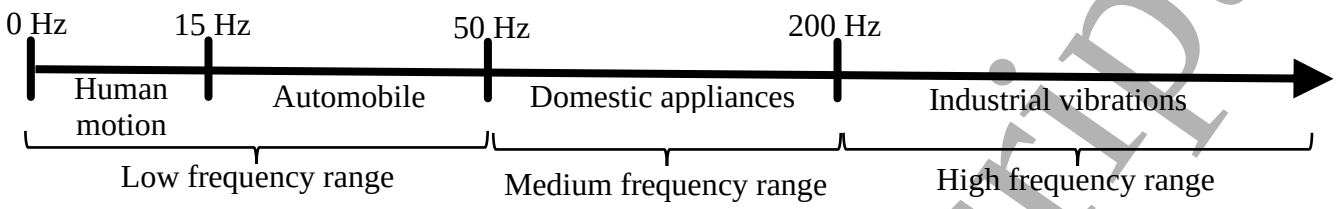

Fig. 1 Operating frequencies of different mechanical energy sources [2]

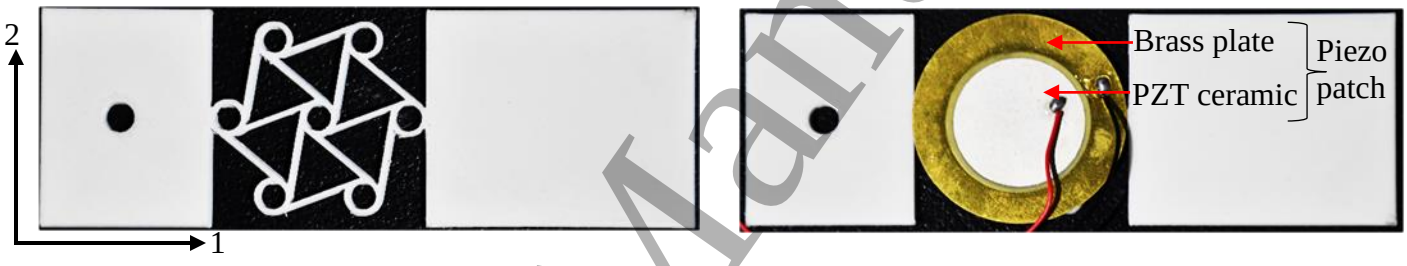

(a) (b)

Fig. 2 Auxetic hexachiral energy harvester (a) substrate (b) substrate with piezo patch

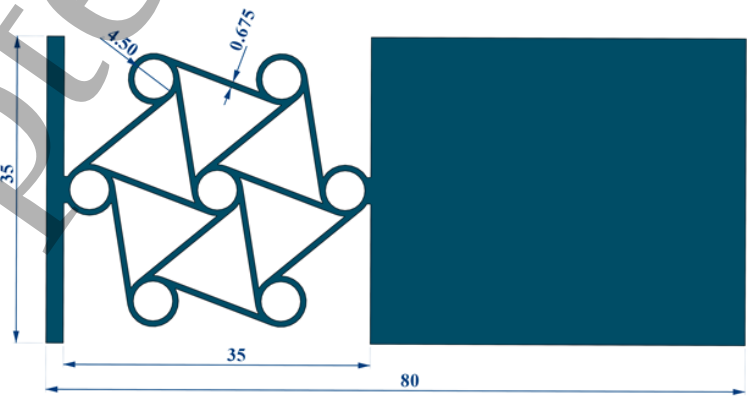

Fig. 3 Geometry of the hexachiral energy harvester (dimensions in mm)

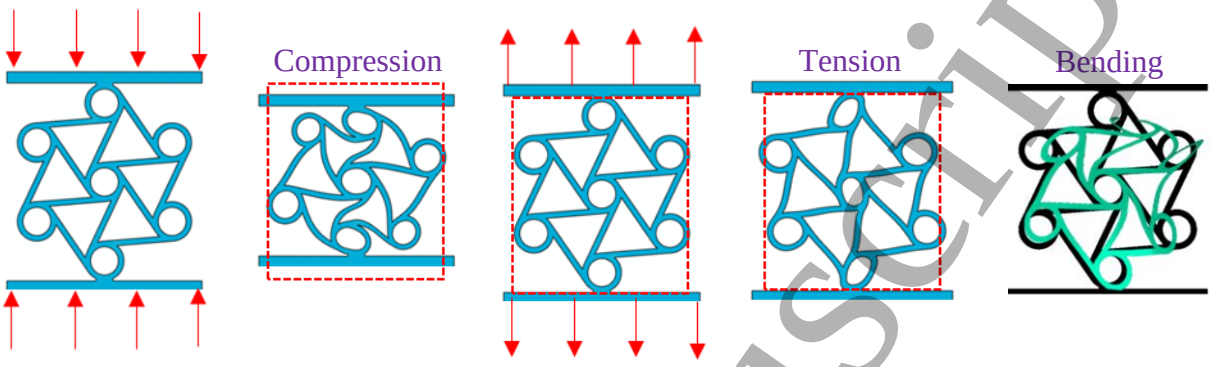

Fig. 4 The response of hexachiral geometry under axial and transverse loading

(a) (b)

Fig. 5 Average stress distribution under uniaxial compression in the piezo patch along (a) axis 1 (b) axis 2

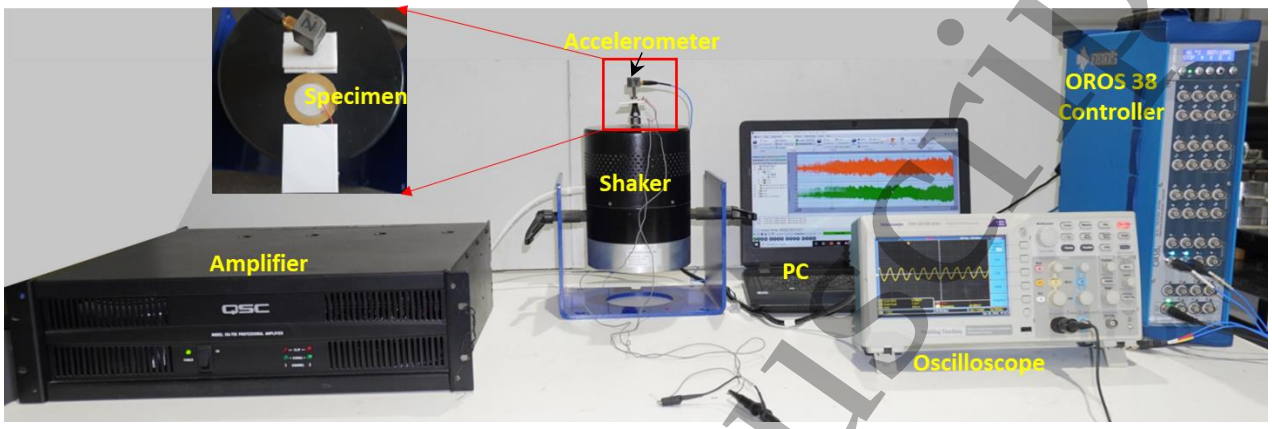

Fig. 6 Experimental setup

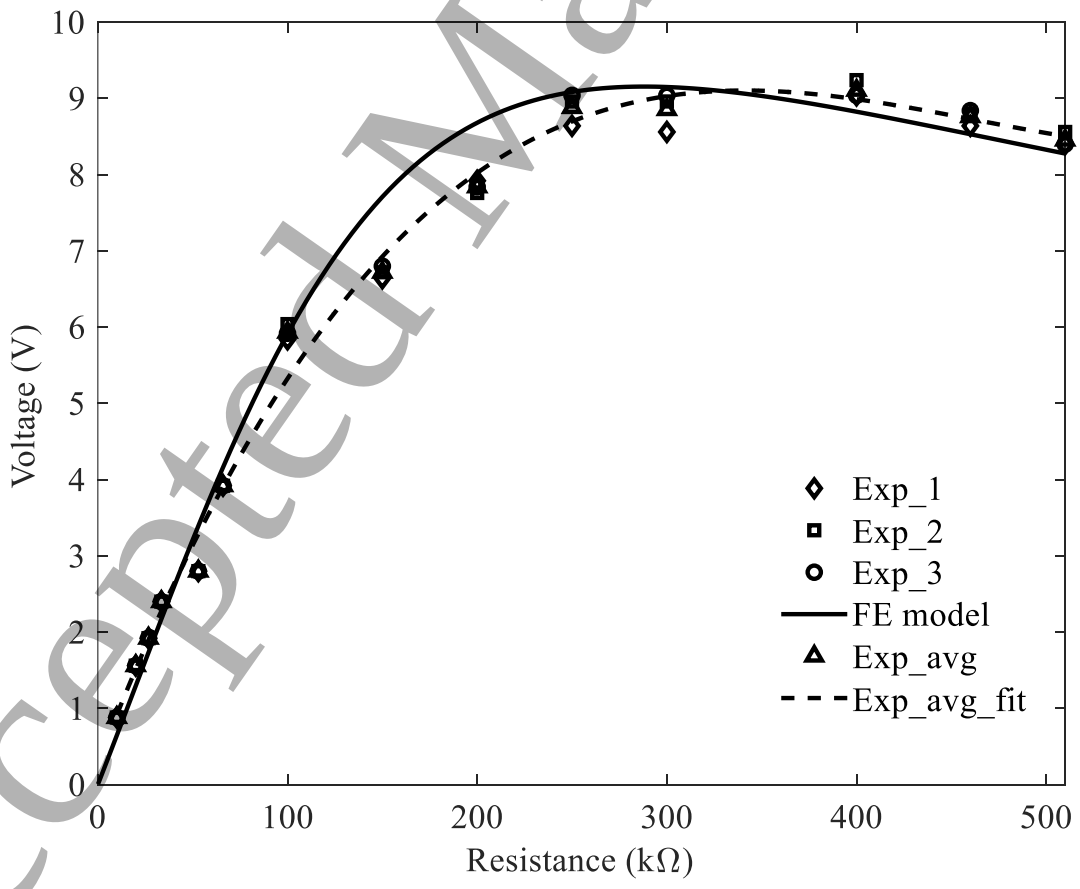

(a)

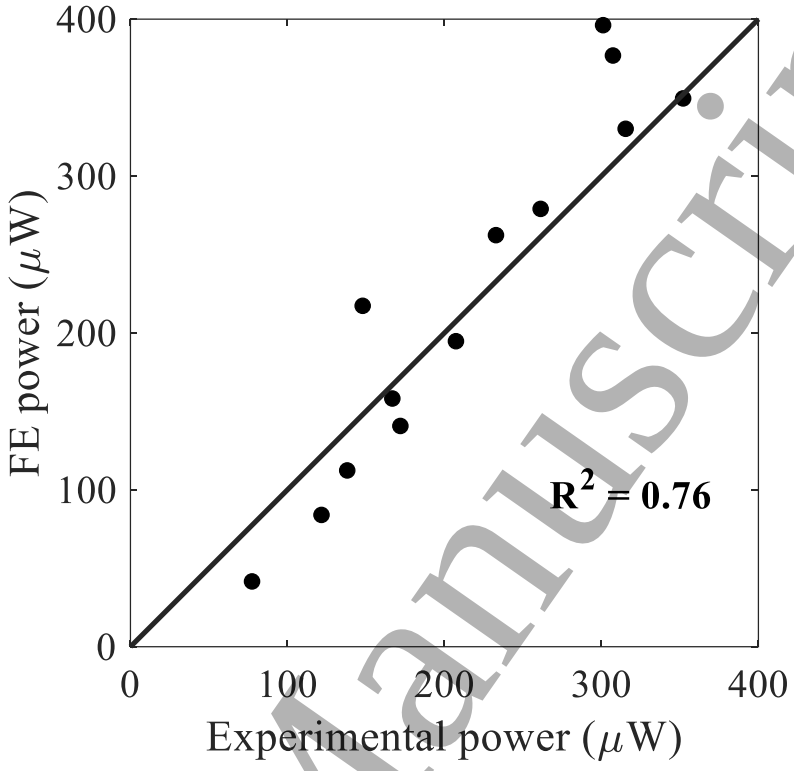

(b)

Fig. 7 Comparison of (a) output voltage and (b) power from experiment and FE model for the hexachiral energy harvester

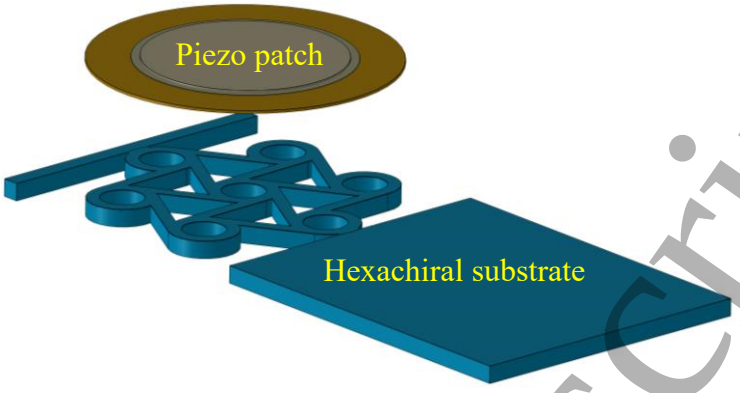

Fig. 8 Exploded view of the hexachiral energy harvester

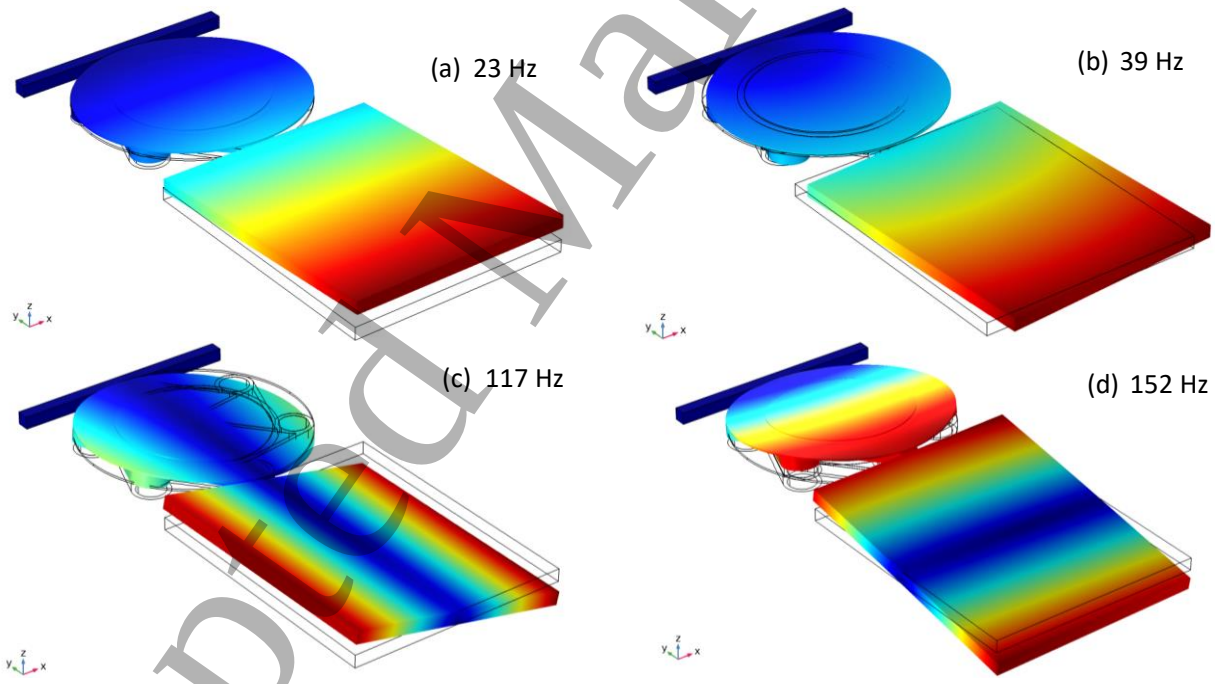

Fig. 9 Natural frequencies and mode shapes of hexachiral energy harvester

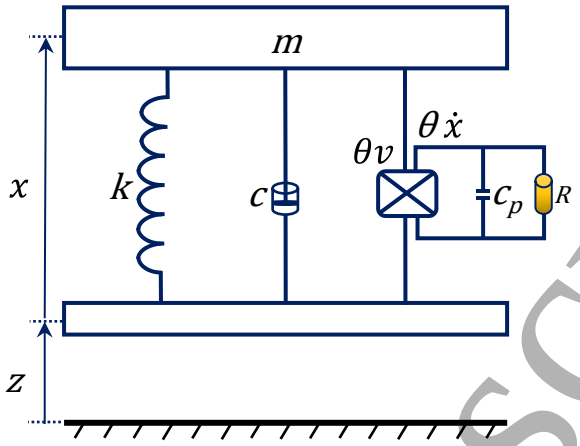

Fig. 10 Schematic of equivalent SDOF model of the hexachiral energy harvester

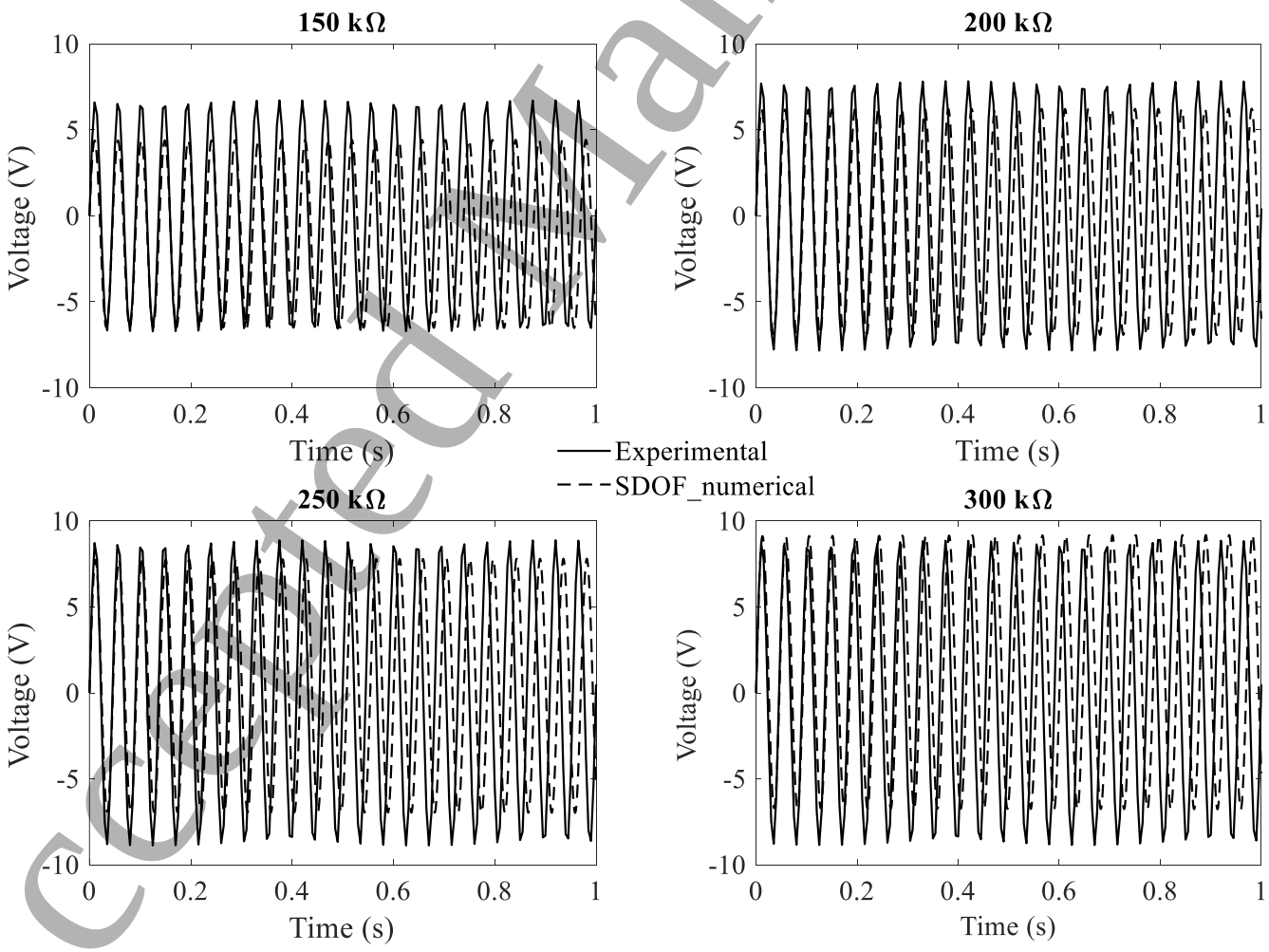

Fig. 11 Comparison of voltage generated by the hexachiral energy harvester at different load resistance

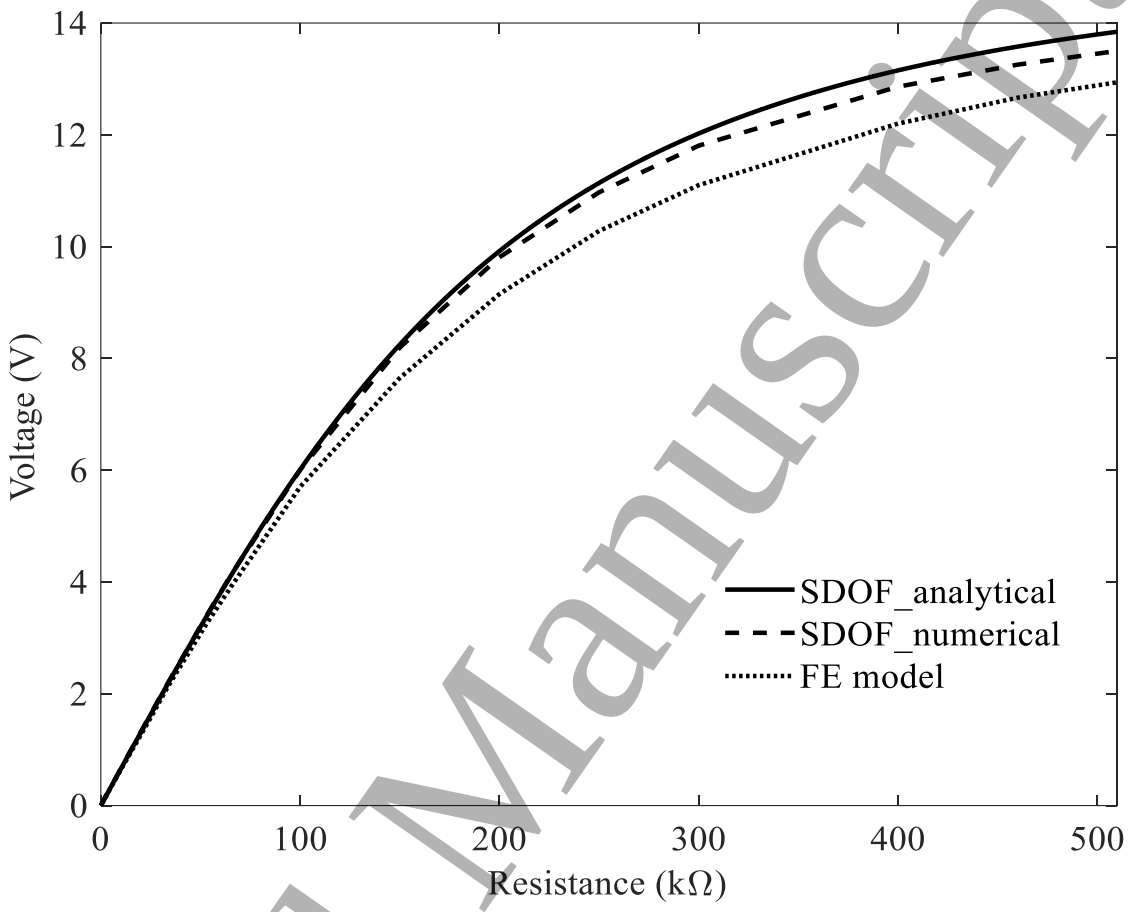

Fig. 12 Comparison of voltage generated by the hexachiral energy harvester at different load resistance

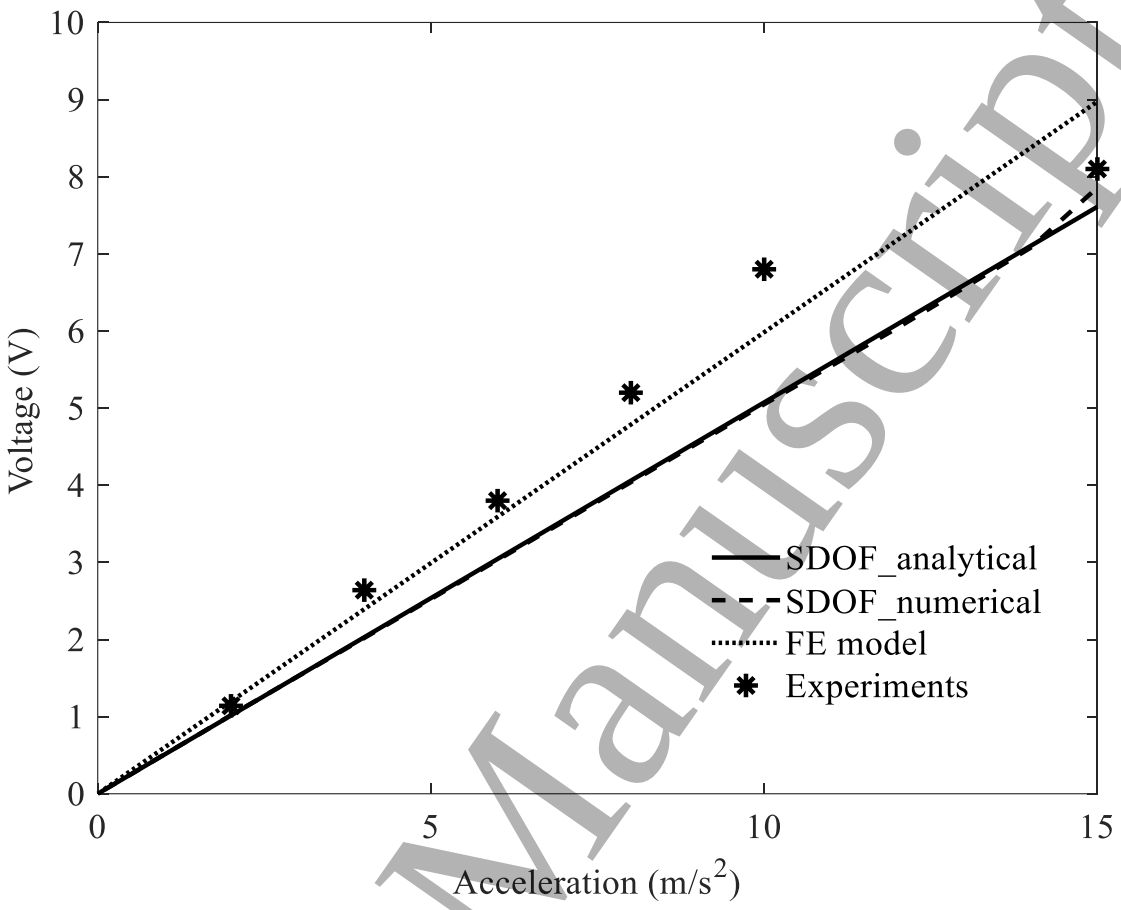

Fig. 13 Comparison of output voltage from experiment, SDOF and FE model for varying base excitation levels

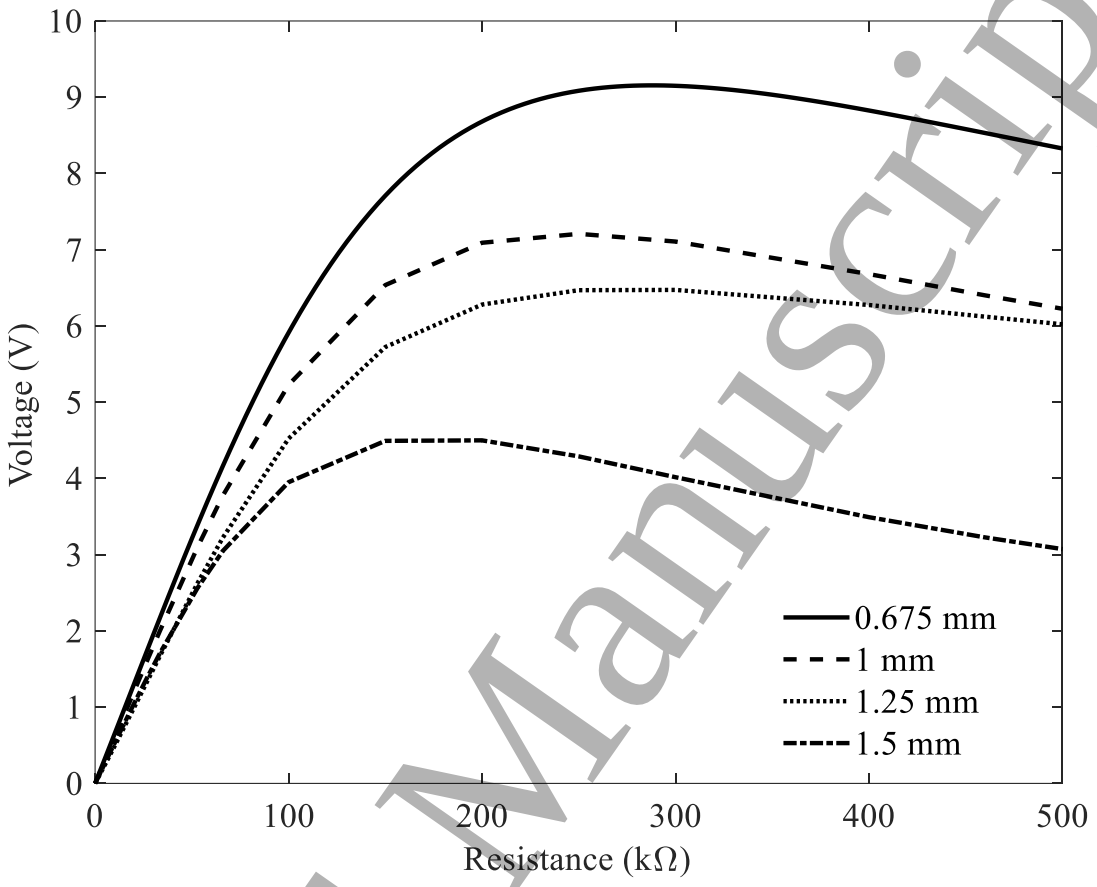

(a)

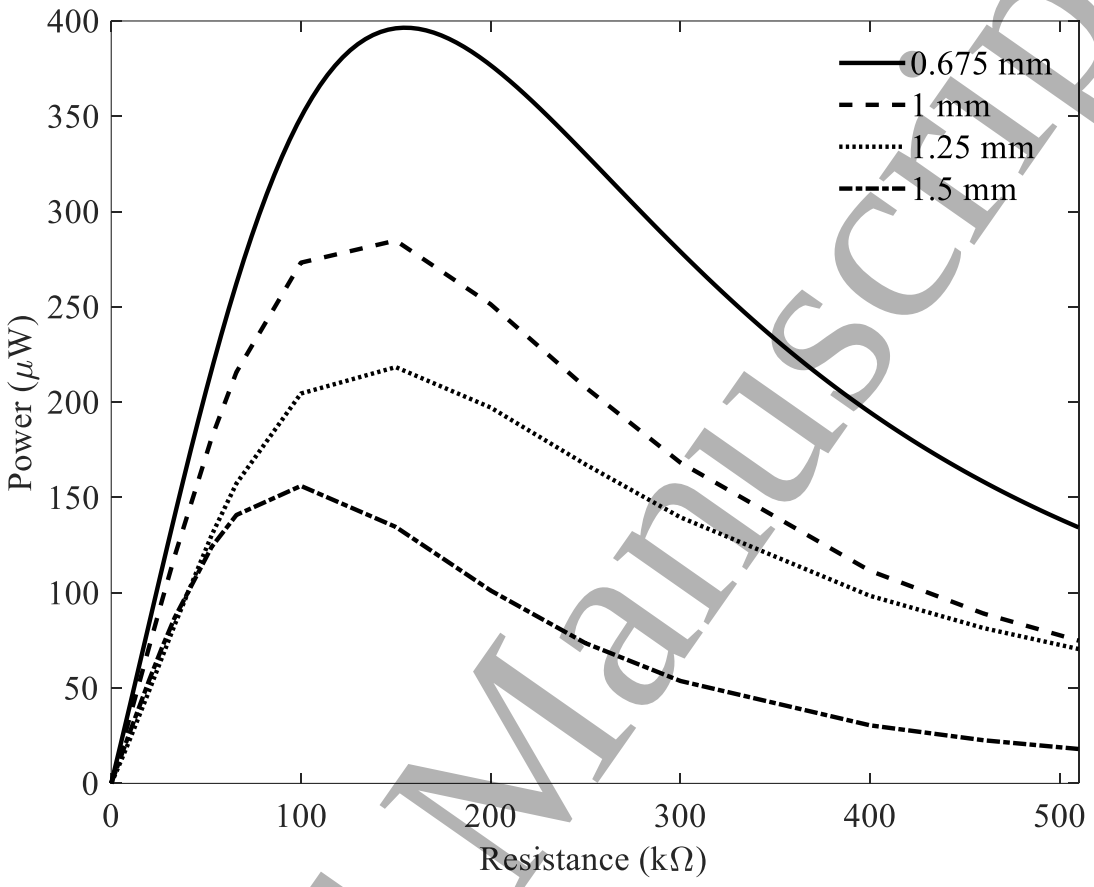

(b)

Fig. 14 Influence of ligament thickness on (a) voltage (b) power output at different resistances

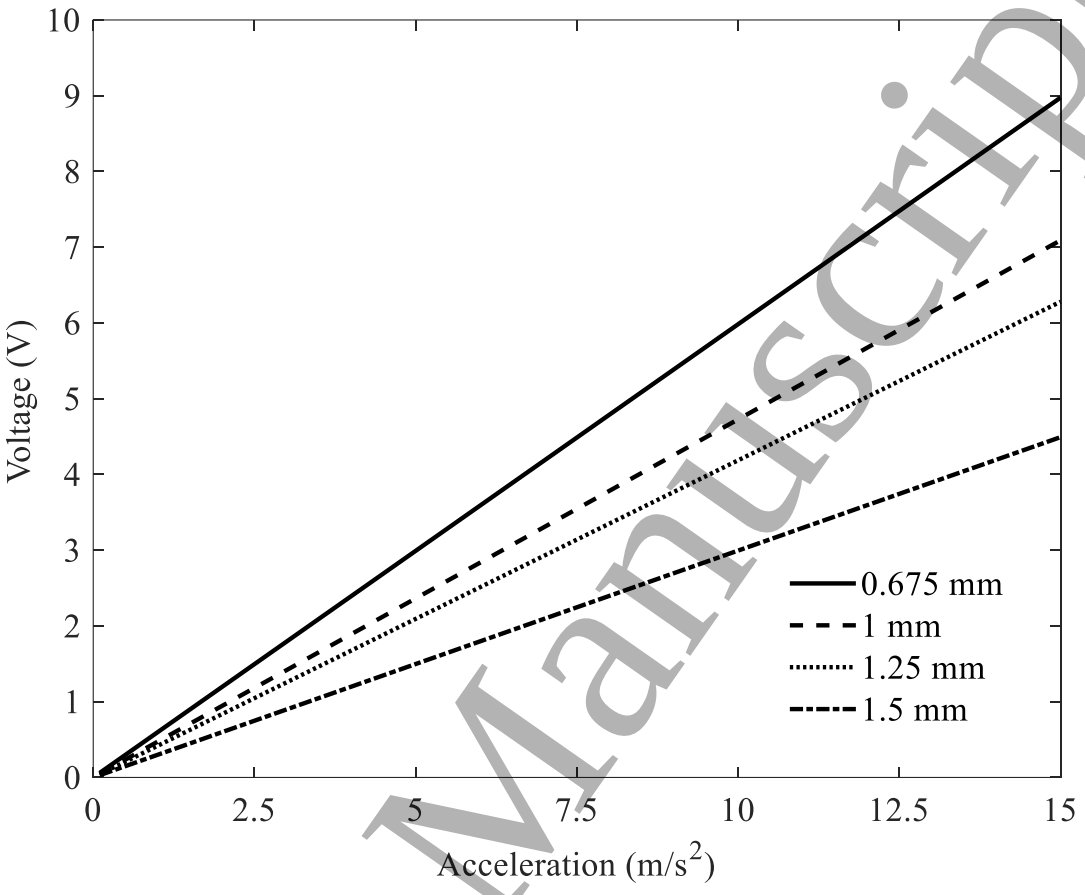

(a)

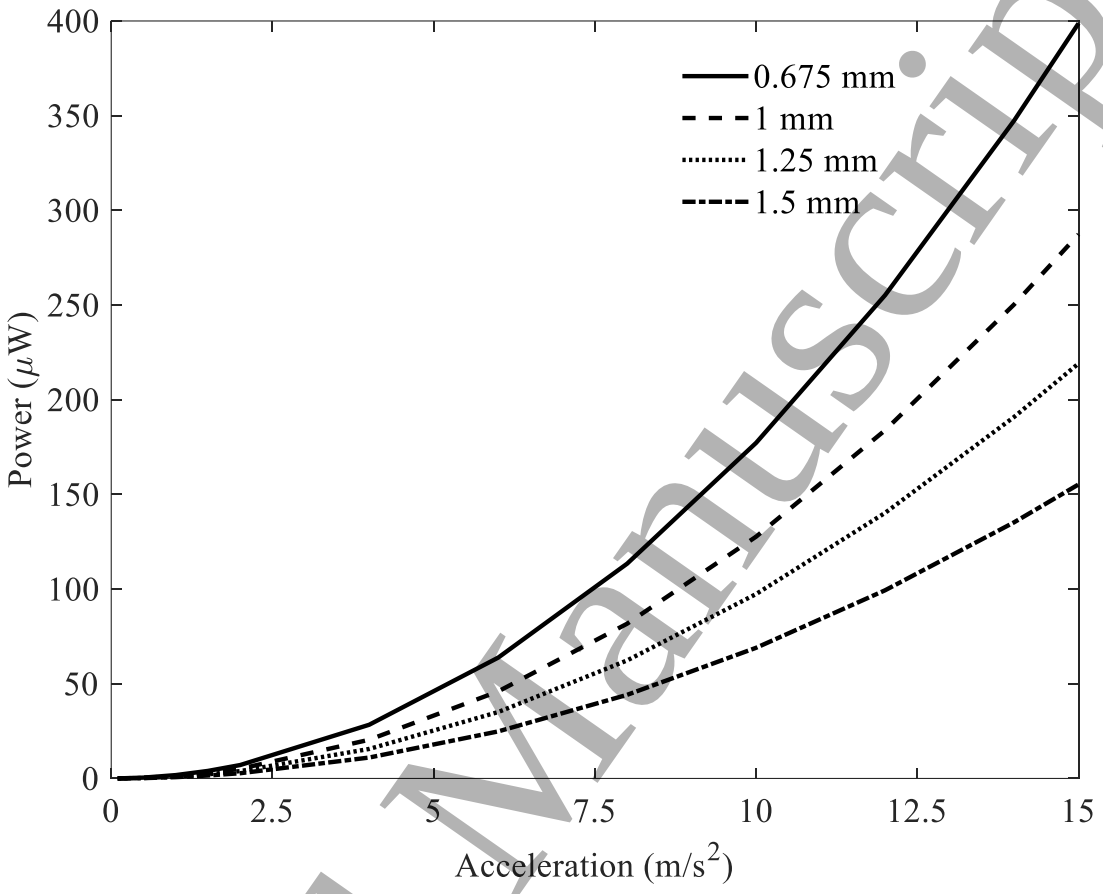

(b)

Fig. 15 Influence of ligament thickness on (a) voltage (b) power at different base excitation levels

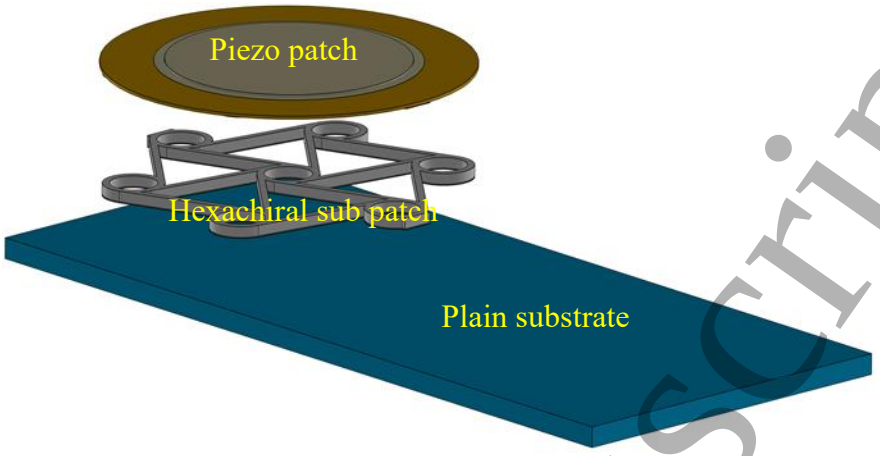

Fig. 16 Exploded view of plain beam energy harvester with hexachiral sub patch

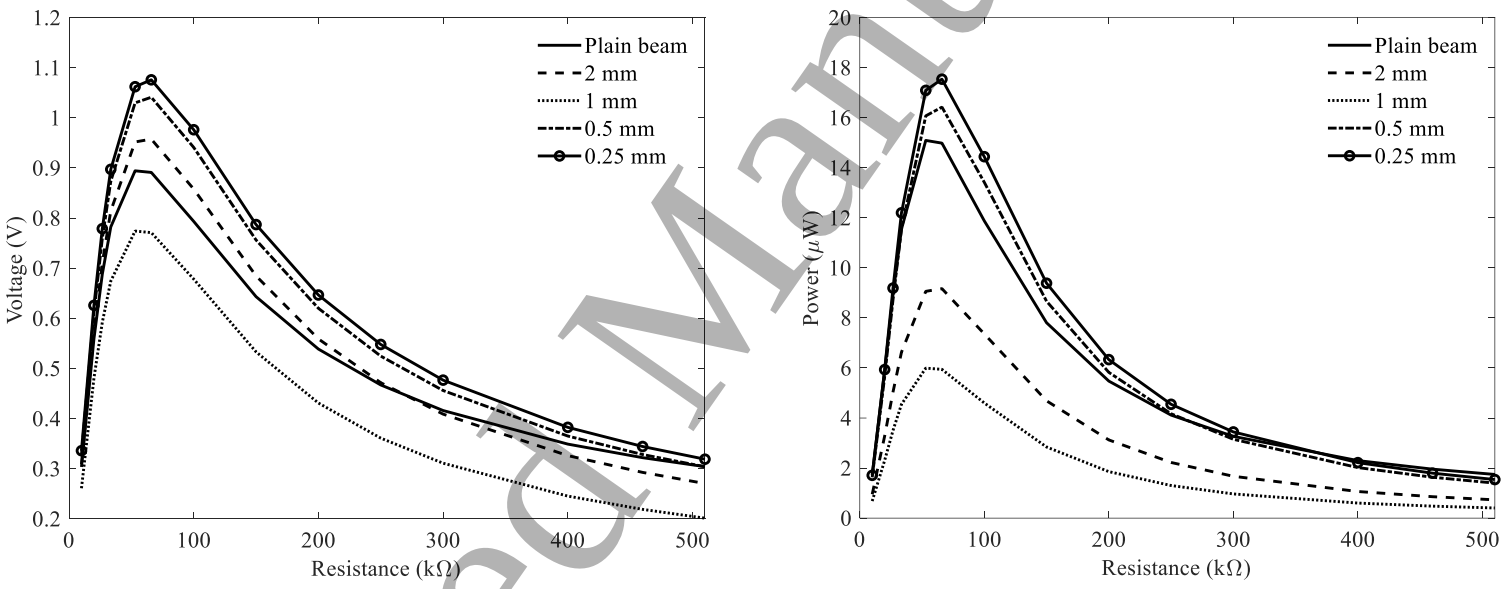

(a) (b)

Fig. 17 Comparison of (a) voltage and (b) power for different resistance

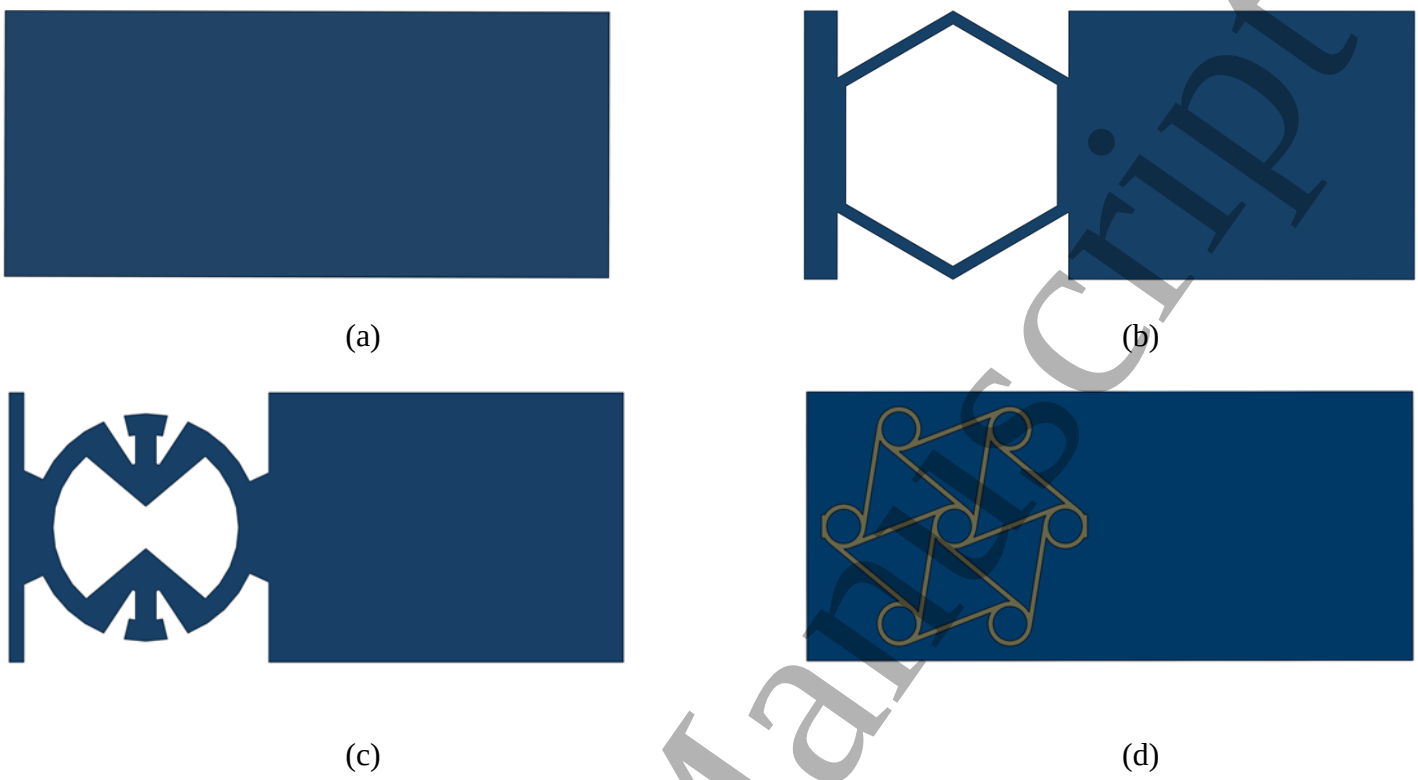

Fig. 18 Harvester designs (a) Plain beam (b) Hexagonal beam (c) Re-entrant beam (d) Plain beam with hexachiral sub patch

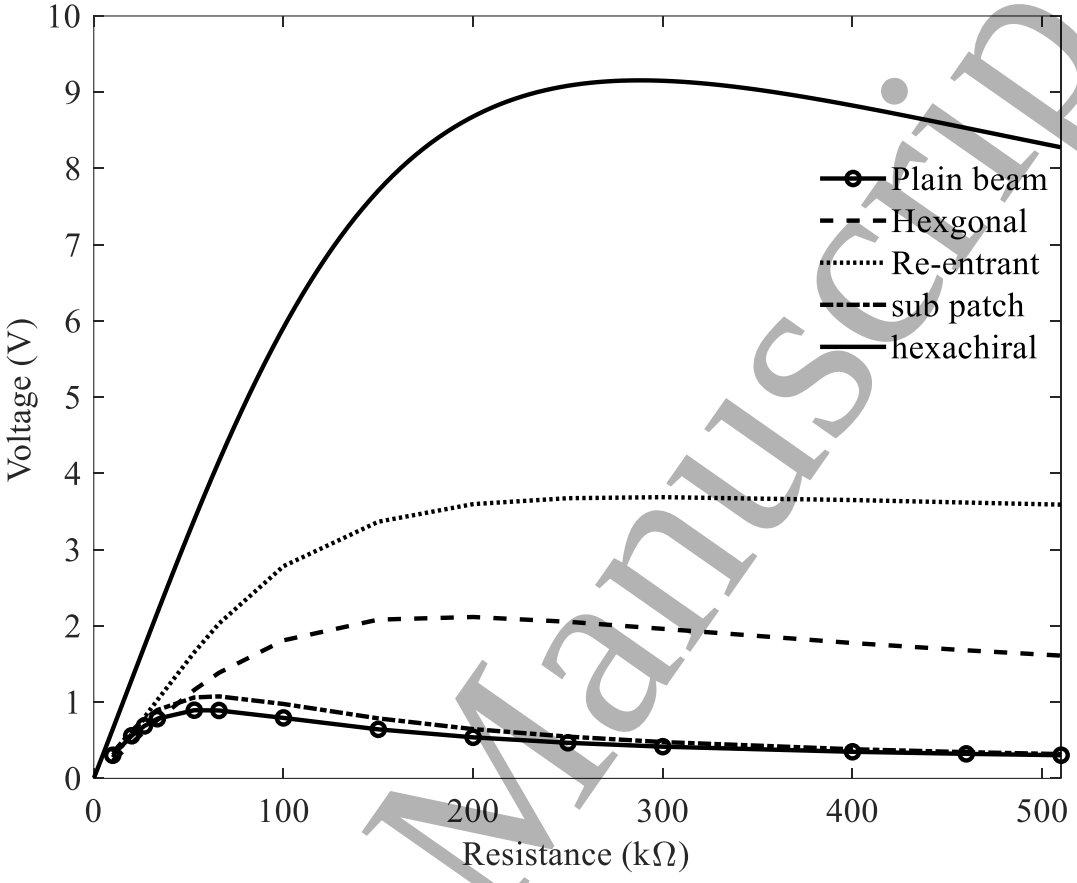

(a)

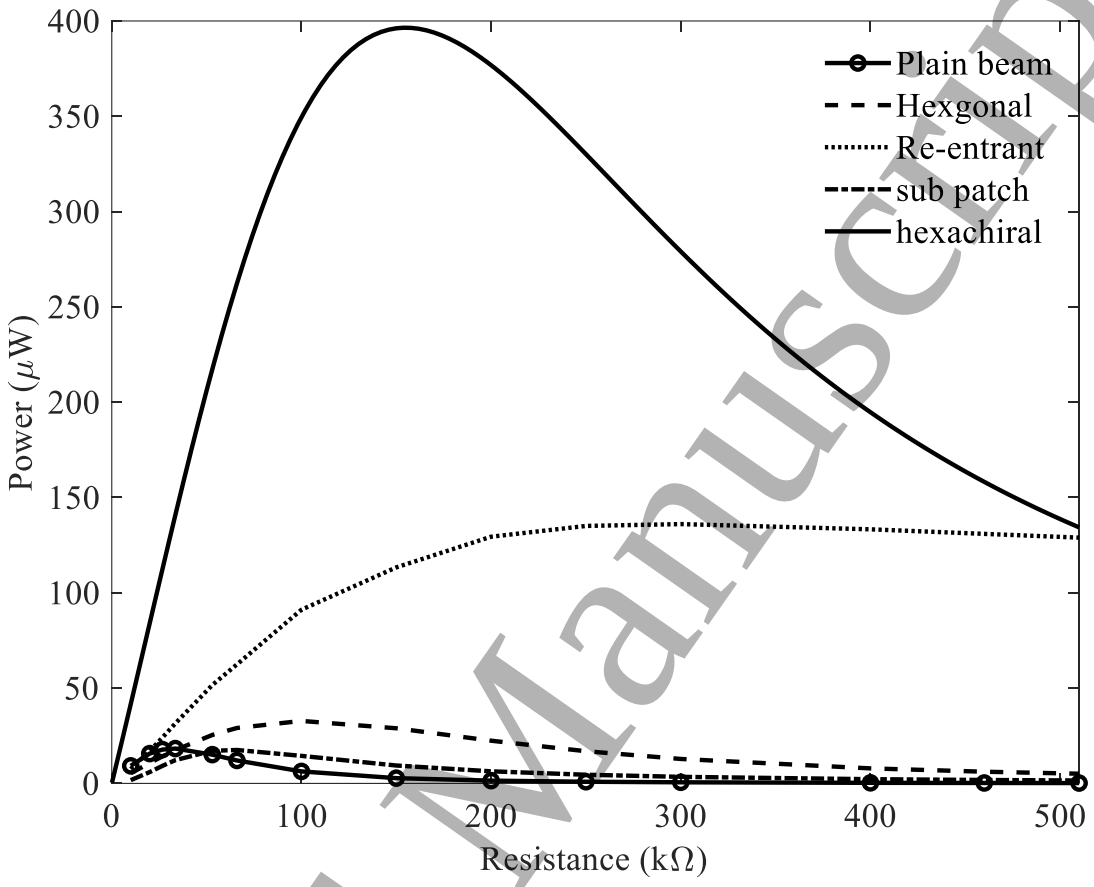

(b)

Fig. 19 Comparison of (a) voltage and (b) power output for different substrate geometries

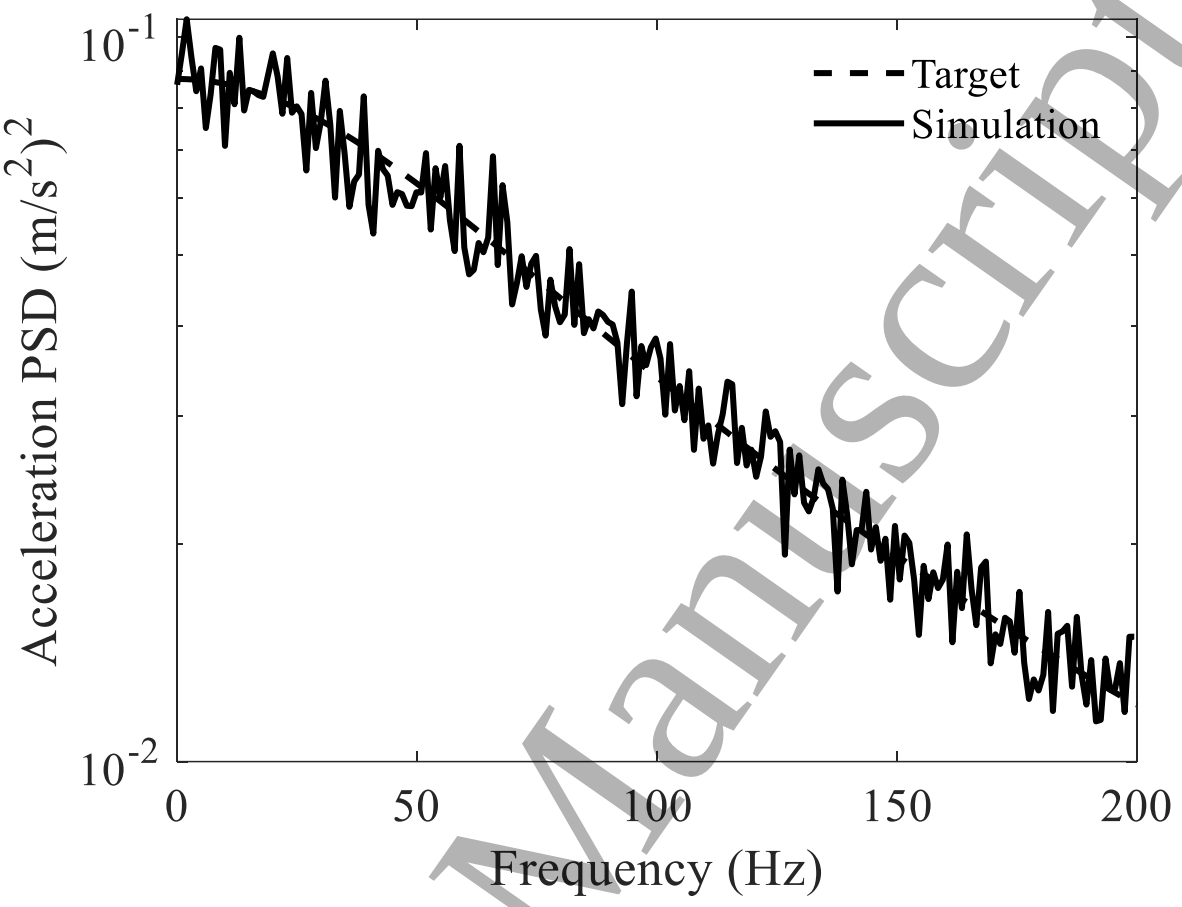

(a)

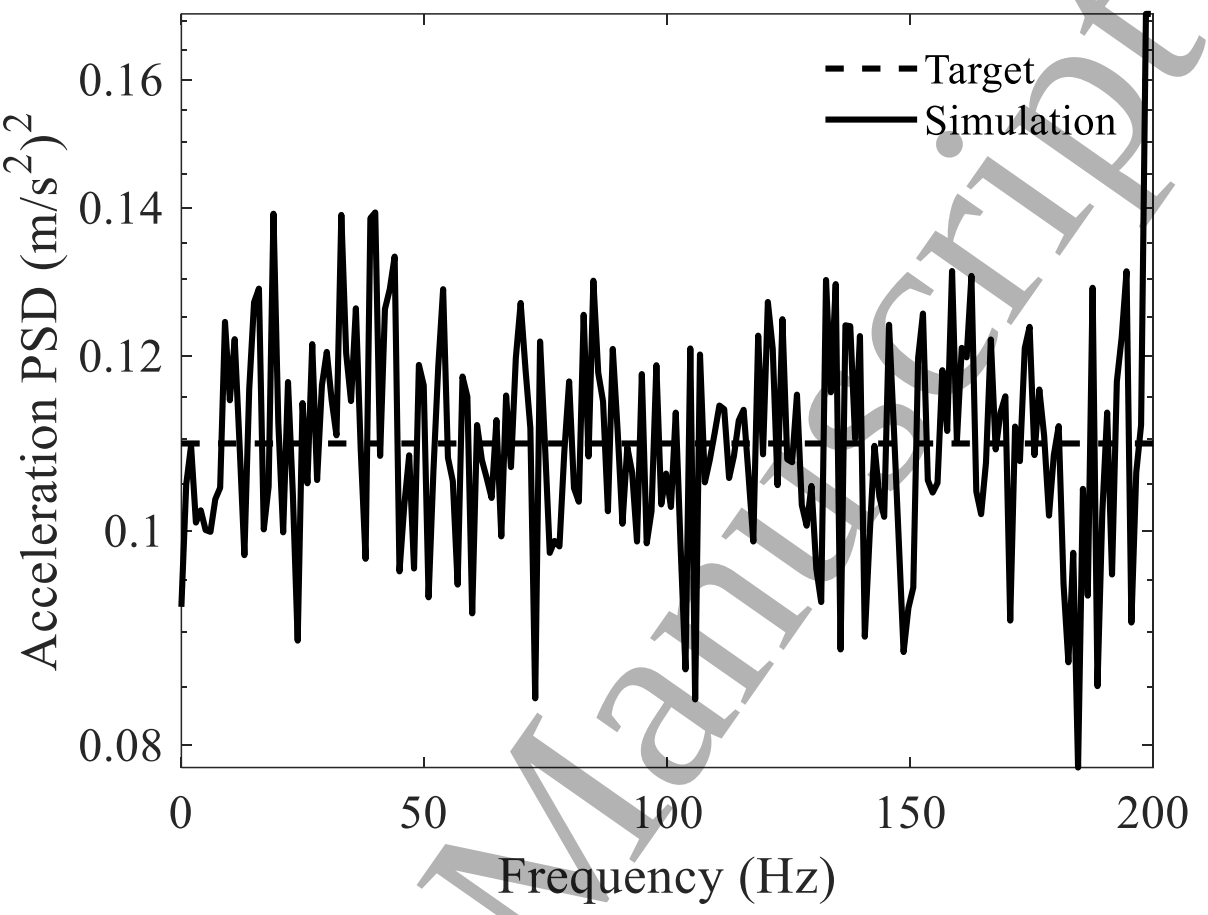

(b)

Fig. 20 Acceleration spectrum of the PSDs considered in the study (a) Variable (b) White noise

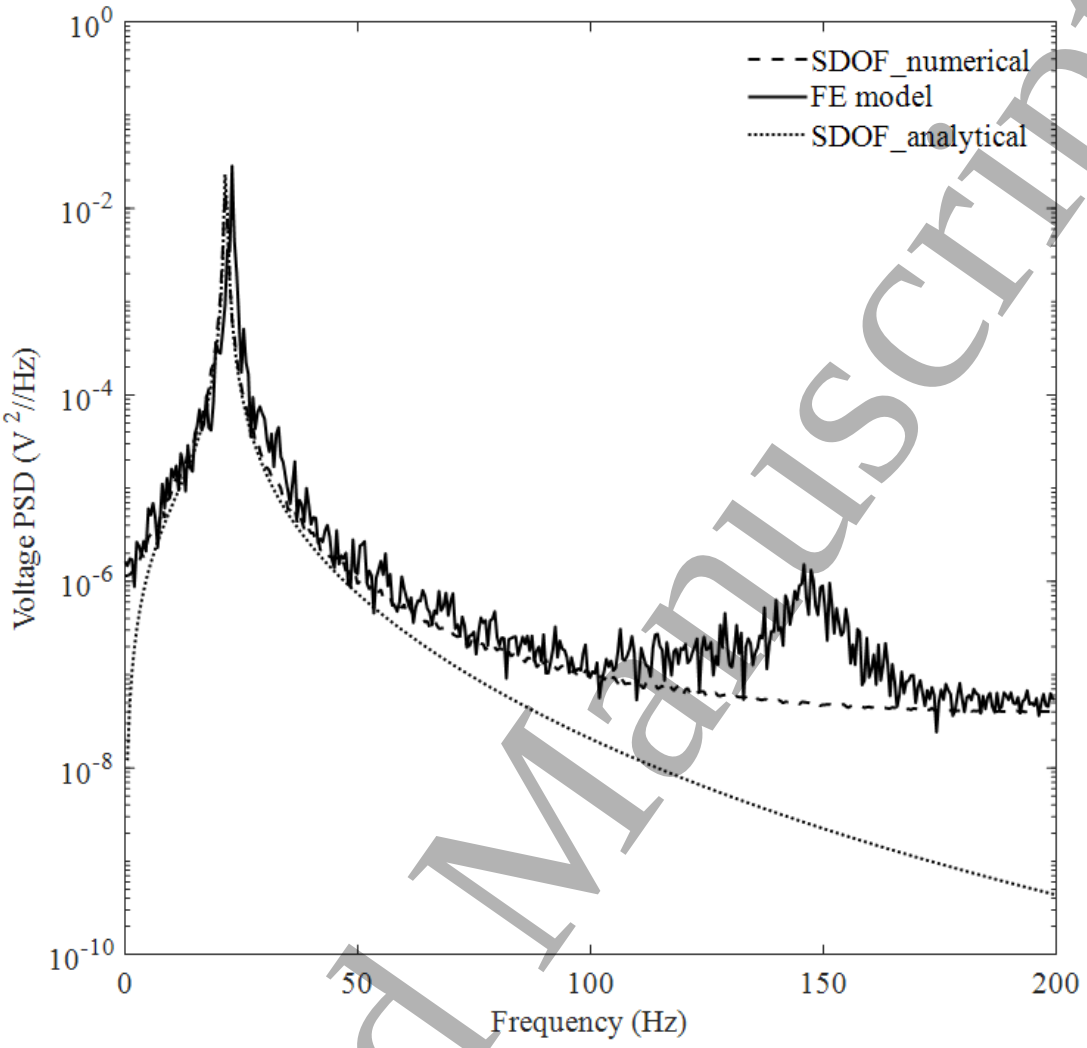

(a)

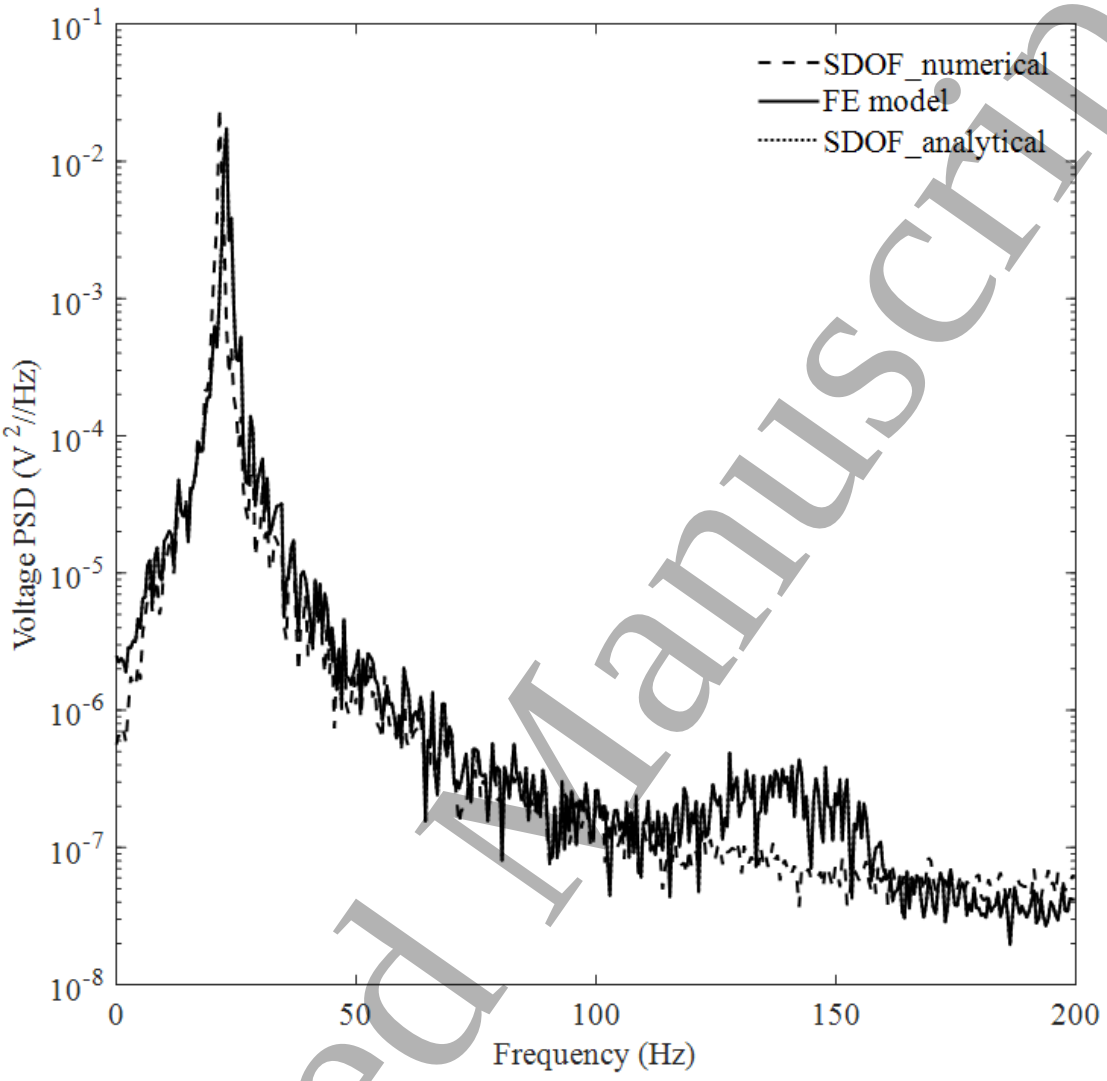

(b)

Fig. 21 Comparison of PSDs obtained from SDOF and FE models for (a) variable (b) constant PSDs

List of Tables

Table 1 Geometrical parameters of hexachiral energy harvester

Part	Parameter	Symbol	Value (mm)
Cantilever resonator	Length	L_b	80
	Width	W_b	35
	Thickness	t_b	2
Epoxy layer 1	Radius	R_{e1}	17.5
	Thickness	t_{e1}	30×10^{-3}
Brass	Radius	R_{br}	17.5
	Thickness	t_b	0.3
Epoxy layer 2	Radius	R_{e2}	17.5
	Thickness	t_{e2}	30×10^{-3}
Piezoelectric layer	Radius	R_p	13.5
	Thickness	t_p	0.2

Table 2 Material properties used in the FE model

Material	Property	Symbol	Value	Unit
PLA	Density	ρ_{PLA}	1230	kg/m^3
	Poisson's ratio	ν_{PLA}	0.36	
	Young's modulus	E_{PLA}	3	GPa
Epoxy	Density	ρ_e	1250	kg/m^3
	Poisson's ratio	ν_e	0.35	
	Young's modulus	E_e	1	GPa
Brass	Density	ρ_b	8490	kg/m^3
	Poisson's ratio	ν_b	0.31	
	Young's modulus	E_b	97	GPa
Lead Zirconate Titanate (PZT-5A): (Piezo patch)	Density	ρ_p	7750	kg/m^3
	Compliance matrix	s_{11}^E	1.64×10^{-11}	1/Pa
		s_{12}^E	-5.74×10^{-12}	1/Pa
		s_{22}^E	1.64×10^{-11}	1/Pa
		s_{13}^E	-7.22×10^{-12}	1/Pa
		s_{23}^E	-7.22×10^{-12}	1/Pa
		s_{33}^E	1.88×10^{-11}	1/Pa
		s_{44}^E	4.75×10^{-11}	1/Pa
		s_{55}^E	4.75×10^{-11}	1/Pa
		s_{66}^E	4.43×10^{-11}	1/Pa
	Coupling matrix	d_{31}	-1.71×10^{-10}	C/N
		d_{32}	-1.71×10^{-10}	C/N
		d_{33}	3.74×10^{-10}	C/N
		d_{24}	5.84×10^{-10}	C/N
		d_{15}	5.84×10^{-10}	C/N
	Relative permittivity	ε_{11}	1730	
		ε_{22}	1730	
		ε_{33}	1700	

Table 3 Parameters used in the SDOF model

Parameter (Symbol)	Value (Units)
Stiffness (k)	136.40 (N/m)
Mass (m)	7.50 (g)
Damping coefficient (c)	0.02 (Ns/m)
Capacitance (c_p)	36.20 (nF)
Coupling coefficient (θ)	9.5×10^{-4} (N/V)

Table 4 Comparison of natural frequencies for hexachiral substrate with different ligament thickness

Ligament thickness (mm)	Mass (g)	Natural frequency (Hz)	Stiffness (N/m)
0.675	7.4	23	137
1.00	7.6	27	167
1.25	7.7	30	182
1.50	7.9	32	201

Table 5 Influence of brass and piezo layer thickness on energy harvester's performance

Thickness (mm)	Brass layer (0.2 mm Piezo layer)		Piezo layer (0.3 mm Brass layer)	
	Frequency (Hz)	Power (μW)	Frequency (Hz)	Power (μW)
0.001	17.2	11	22.8	<10
0.1	19.1	331	19.1	567
0.2	20.9	415	20.9	397
0.3	23.0	397	23.0	217
0.4	24.6	202	-	-
0.5	25.5	109	-	-

Table 6 Natural frequencies of a plain beam harvester with hexachiral sub patch

Sub patch thickness (mm)	Natural frequency (Hz)
0	97
0.25	85
0.50	86
1	88
2	91

Table 7 Performance of harvesters with different substrate geometries

Beam geometry	Natural frequency (Hz)	Optimum resistance (kΩ)	Voltage (V)	Power (μW)
Plain	97	53	0.9	15
Re-entrant	45	300	3.7	137
Hexagonal	35	150	2.1	29
Hexachiral	23	154	7.8	397
Hexachiral sub patch	85	66	1.1	17.5

Table 8 Spectral moments of the voltage PSD for variable and constant acceleration PSDs

Methods	Variable PSD		Constant PSD	
	Mean	Variance	Mean	Variance
SDOF_ode45	21.58	3.50	21.60	3.16
SDOF_analytical	21.61	2.12	21.63	2.24
FE Model	22.94	3.50	22.89	4.75